Sliding Distance per ATP Molecule Hydrolyzed by Myosin Heads during Isotonic Shortening of Skinned Muscle Fibers

Hideo Higuchi* and Yale E. Goldman
Department of Physiology and Pennsylvania Muscle Institute, University of Pennsylvania, Philadelphia, PA 19104-6083

ABSTRACT We measured isotonic sliding distance of single skinned fibers from rabbit psoas muscle when known and limited amounts of ATP were made available to the contractile apparatus. The fibers were immersed in paraffin oil at 20°C, and laser pulse photolysis of caged ATP within the fiber initiated the contraction. The amount of ATP released was measured by photolyzing ^{3}H-ATP within fibers, separating the reaction products by high-pressure liquid chromatography, and then counting the effluent peaks by liquid scintillation. The fiber stiffness was monitored to estimate the proportion of thick and thin filament sites interacting during filament sliding. The interaction distance, D_i, defined as the sliding distance while a myosin head interacts with actin in the thin filament per ATP molecule hydrolyzed, was estimated from the shortening distance, the number of ATP molecules hydrolyzed by the myosin heads, and the stiffness. D_i increased from 11 to 60 nm as the isotonic tension was reduced from 80% to 6% of the isometric tension. Velocity and D_i increased with the concentration of ATP available. As isotonic load was increased, the interaction distance decreased linearly with decrease of the shortening velocity and extrapolated to 8 nm at zero velocity. Extrapolation of the relationship between D_i and velocity to saturating ATP concentration suggests that D_i reaches 100–190 nm at high shortening velocity. The interaction distance corresponds to the sliding distance while cross-bridges are producing positive (working) force plus the distance while they are dragging (producing negative forces). The results indicate that the working and drag distances increase as the velocity increases. Because D_i is larger than the size of either the myosin head or the actin monomer, the results suggest that for each ATPase cycle, a myosin head interacts mechanically with several actin monomers either while working or while producing drag.

INTRODUCTION

Muscle contracts by relative sliding of thin and thick filaments driven by the interaction of myosin heads with actin coupled to hydrolysis of ATP (A. F. Huxley and Niedergerke, 1954; H. E. Huxley and Hanson, 1954; A. F. Huxley, 1957; Cain et al., 1962). The mechanical impulse of the actomyosin interaction has been assumed to result from a shape change or tilting motion of the 19-nm-long myosin heads (Elliott and Offer, 1978) projecting from the thick filament while attached to actin in the thin filaments (Reedy et al., 1965; H. E. Huxley, 1969; A. F. Huxley and Simmons, 1971; Rayment et al., 1993). This motion would produce ~12 nm of filament sliding (A. F. Huxley and Simmons, 1971; Ford et al., 1977). If each tilting motion is coupled with hydrolysis of an ATP molecule by a myosin head, the working stroke per ATP molecule hydrolyzed would be 10–20 nm (A. F. Huxley, 1957; H. E. Huxley, 1969; Lymn and Taylor, 1971). A crucial problem in the muscle field, and also generally in biology, is whether biological transduction operates by tight or loose coupling mechanisms (Oosawa and Hayashi, 1986). Whether hydrolysis of an ATP molecule is coupled tightly to one mechanical motion or to several motions (loose coupling) might be addressed by measuring the length of the working stroke.

In A. F. Huxley's (1957) model of the contraction mechanism, cross-bridges between the two sets of filaments cycle between attachment and detachment, and they produce both positive (working) and negative (drag) forces during sliding. The force generated by a muscle is the difference between these working and drag components. Huxley estimated the working distance per cross-bridge cycle to be ~16 nm from the results of heat measurements by Hill (1938). In the 1957 model, the average drag distance at maximum velocity is the same as the working distance to give zero net force.

From measurements of sliding velocity and ATPase activity of myofibrils, Yanagida and colleagues (1985) estimated the working distance per ATP molecule hydrolyzed to be ≥60 nm at zero load. Estimates of the sliding distance per ATP molecule hydrolyzed from in vitro assays of actomyosin motility have varied from 8 nm (Toyoshima et al., 1990) to 10–28 nm (Uyeda et al., 1990, 1991) to >200 nm (Harada et al., 1990). These values correspond to either the working stroke or the working plus the drag strokes in the various experiments. Sliding of more than ~40 nm per ATP molecule hydrolyzed is incompatible with tight coupling between the ATPase and mechanical cycles.

The estimates of the working (+ drag) distance from experiments on myofibrils and in vitro motility assays probably vary so widely because very indirect estimates are used for several crucial parameters: the number of myosin heads interacting with the actin filament and in some cases the number of ATP molecules hydrolyzed. Working distance in

Received for publication 7 March 1995 and in final form 6 July 1995.

Address reprint requests to Yale E. Goldman, Department of Physiology, University of Pennsylvania School of Medicine, D700 Richards Building, 3700 Hamilton Walk, Philadelphia, PA 19104-6083. Tel.: 215-898-4017; Fax: 215-898-2653; E-mail: goldman@a1.mscf.upenn.edu.

*Present address: Yanagida BioMotron Project, 2–4-14 Senba-Higashi, Mino, Osaka 562, Japan.

0006-3495/95/10/1491/17 $2.00

relation to ATPase activity has been estimated in vitro only at zero load. Muscle fibers have some advantages in regard to these factors. Physiological loads can be applied during shortening, and the number of cross-bridges attached to the thin filaments at a given time can be estimated from the mechanical stiffness (A. F. Huxley and Simmons, 1973). The number of ATP molecules hydrolyzed per myosin head can be calculated in skinned muscle fibers from the concentration of ATP used.

In this work we measured the isotonic sliding distance during the interaction between myosin and actin per ATP molecule made available by photolysis of caged ATP within single skinned fibers of rabbit muscle. In an earlier study (Higuchi and Goldman, 1991b) and in preliminary reports (Higuchi and Goldman, 1991a, 1992) using the same approach, we obtained an interaction distance at low loads, suggesting multiple mechanical interactions per ATPase cycle. Here we document the techniques, present data over a wider range of conditions, and discuss various types of actomyosin states that may contribute to the interaction distance.

MATERIALS AND METHODS

Calculation of the interaction distance

We term the isotonic sliding distance per ATP molecule hydrolyzed by myosin heads interacting with actin filaments the interaction distance, D_i (Higuchi and Goldman, 1991b). A limited amount of ATP was made available to the contractile apparatus by photolyzing caged ATP. The number (N_i) of ATP molecules hydrolyzed per myosin head in the fiber can be calculated from the concentration ($[ATP_u]$) of ATP molecules used by actomyosin divided by the concentration ($[M_i]$) of myosin heads interacting simultaneously with actin filaments in the fiber: $N_i = [ATP_u]/[M_i]$. $[M_i]$ is equal to the total concentration ($[M_o]$) of myosin heads in the fiber multiplied by the proportion (S_a) of heads interacting simultaneously with actin: $[M_i] = S_a \cdot [M_o]$. D_i was thus calculated as

$$D_i = \frac{D_s}{N_i} = \frac{D_s \cdot [M_i]}{[ATP_u]} = \frac{D_s \cdot S_a \cdot [M_o]}{[ATP_u]} \quad (1)$$

where D_s is the total sliding distance determined as shortening per half sarcomere. S_a was estimated from the average stiffness at 500 Hz during shortening relative to that in rigor at full overlap between the thick and thin filaments, assuming that the stiffness of the fiber is proportional to the number of actomyosin cross-bridges (A. F. Huxley and Simmons, 1973; Ford et al., 1981). The effect of filament compliance (H. E. Huxley et al., 1994; Wakabayashi et al., 1994; Higuchi et al., 1995) on the estimate of S_a is considered in the Discussion section. $[M_o]$ was assumed to be 154 μM (Ferenczi et al., 1984), as determined under conditions similar to ours. Therefore, to estimate D_i we measured the concentration ($[ATP_u]$) of ATP used in the fiber, the sliding distance (D_s), and the average stiffness (S_a).

Fiber preparation and mechanical measurements

Glycerol-extracted single fibers from rabbit psoas muscle were prepared, as described by Goldman et al. (1984a). Fibers were stored at −20°C in 50% glycerol for 2–24 days, 7 days on average. The fibers were dissected in silicone oil (Dow Corning Midland, MI; 200 fluid, viscosity 10 cs) at ~10°C. The ends of a fiber segment, ~3 mm in length and ~80 μm in diameter, were attached horizontally with T-shaped aluminum clips to hooks from a strain-gauge tension transducer (AE801, Akers, Horten, Norway) (Goldman and Simmons, 1984) and a linear moving-coil motor kindly supplied by Dr. V. Lombardi, University of Florence (Cecchi et al., 1976). The resonant frequencies of the tension transducer and the motor were ~5 and 3 kHz, respectively.

Fibers were activated from rigor by photolysis of caged ATP in the presence of Ca^{2+} (Goldman et al., 1984b). The fiber was held at fixed length during the photolysis laser pulse; after liberation of ATP, force increased toward the active tension level. When a preset force level was reached, the error signal for the motor was switched by a controller similar to the "diode switching network" described by Gordon et al. (1966) to clamp force at a constant value. The fiber then shortened isotonically. In isotonic mode, the feedback gain was ~50 and rolled off above 200 Hz. Length oscillations, 0.2–0.4% strain peak-to-peak at 500 Hz, were applied directly at the motor power amplifier for measurement of stiffness.

Optical components and data recording

The light source for photolysis of caged ATP was a ~50-ns pulse from a frequency-doubled ruby laser, λ = 347 nm (Goldman et al., 1984a). The collimated 347-nm beam generated by the laser was circular in cross-section with a diameter of 11 mm. The beam was compressed in the vertical direction to ~3 mm by a cylindrical fused silica lens.

The sarcomere length of a central region of the fiber, ~2 mm in length, was measured by a white light diffraction method (Goldman, 1987b) that avoids the Bragg-angle artifact present in laser diffraction experiments. Temporal and spatial resolution of the sarcomere length signals were 60 μs and 0.1 nm per half sarcomere, respectively.

Tension and position of the motor were continuously monitored on a chart recorder. The tension, position of the motor, and sarcomere length signals were digitized at 0.5–1 kHz sampling rate and stored on diskettes by a Z-80-based microcomputer. Tension and shortening distance were measured from the digitized records using locally developed software. For stiffness measurements, the tension and sarcomere length were separately recorded at 20 kHz sampling rate on a digital storage oscilloscope (model 3091, Nicolet, Madison, WI), transferred to an 80286-based personal computer, and stored on diskettes. The 500-Hz sinusoidal components of the tension and sarcomere length signals were isolated from the 20-kHz recordings by passage through 500 Hz, Q = 2 digital, recursive, band-pass filters (Rader and Gold, 1967). Stiffness was taken as the ratio of amplitudes of the 500-Hz component of the tension to that of the sarcomere length signal.

Solutions and trough

Caged ATP was synthesized as in Walker et al. (1988). The proportion of contaminant ADP in the caged ATP was <0.1%. The concentration of caged ATP was determined from its absorption coefficient $E_{260\ nm}$ = 19.6 $mM^{-1}\ cm^{-1}$. Tritium-labeled caged ATP (caged ^{3}H-ATP), synthesized as in Ferenczi et al. (1984), was kindly supplied by Dr. E. Homsher, University of California, Los Angeles.

The constituents of the experimental solutions are listed in Table 1. The calculated concentration of free Mg^{2+} was set to 1.0 mM in all solutions, and the calculated free $[Ca^{2+}]$ was 30 μM in Ca-rigor solution. Ionic strength of the solutions was 200 mM. Solutions were mixed at ~20°C and brought to pH 7.1 with KOH. The Ca-rigor solution contained 40 μM of the myokinase inhibitor, diadenosine pentaphosphate (AP_5A) (Sigma, St. Louis, MO).

A stepper motor-driven solution exchanger was used similar to that described in Goldman et al. (1984a). The stainless steel trough assembly had five wells containing various experimental solutions. For solution exchanges, the fiber stayed in place and the trough assembly was lowered, shifted horizontally, and raised to immerse the fiber in the new solution. The fiber was in air for <3 s. The solution in the well containing the fiber could be stirred by moving the trough 200 μm up and down ~5 times per second via a stepper motor. The well (front trough) on the laser end of the trough assembly was made from fused silica windows. After the fiber was

TABLE 1 Solutions used during caged ATP photolysis trials (concentrations in mM)

Solution	Na_2ATP	$MgCl_2$	EGTA	Ca-EGTA	HDTA	TES	GSH	caged-ATP
Relax	1.1	4.1	51	0	0	100	10	0
Rigor	0	3.2	53	0	0	100	10	0
Ca-Rigor	0	1.3	0	20	33	100	10	0.4–4

Abbreviations: EGTA, ethyleneglycol-bis-(β-aminoethylether)N,N,N′,N′-tetraacetic acid; Ca-EGTA, contains the same concentrations of total Ca and EGTA; TES, N-tris(hydroxymethyl)methyl-2-aminoethanesulphonic acid; GSH, reduced glutathione; caged ATP, P^3-1-(2-nitro)phenylethyladenosine 5′-triphosphate; and HDTA, 1,6-diaminohexane-N,N,N′,N′-tetraacetic acid.

transferred to this well, a fused silica cover was added so that the trough was optically clear for the horizontal laser beam and for the vertically directed polychromatic light used to monitor the sarcomere length.

Experimental procedure

Before and after each experiment, the total energy of laser beam and the energy density in the region that illuminated the fiber were measured by using a disc calorimeter (model 36–001/365, Scientech, Boulder, CO) placed before the cylindrical lens. To measure the laser energy illuminating the fiber, a mask with a rectangular slit 0.3 mm in height and 3 mm wide was set in front of the cylindrical lens. The rectangular laser beam propagating through this size slit was compressed by the cylindrical lens to ~80 μm, corresponding to the diameter of a fiber. The position of the mask was adjusted by micrometers until the laser beam traversing the slit was centered on the motor and the tension transducer hooks where the fiber would be mounted. The laser energy was then measured through the slit. The energy falling on the fiber was less than the measured amount because of reflection of ~15% of the energy at the cylindrical lens and entrance window of the trough.

Single fibers were mounted in the experimental trough in the relaxing solution, stretched to 30% above slack length (sarcomere length 2.7–2.9 μm), and then treated for 5–10 min with relaxing solution containing 0.5% Triton X-100 to remove residual membrane components. All procedures were performed at 20 ± 1°C. The fiber was transferred to rigor solution, and the bath was stirred for ~30 s to rapidly wash ATP out of the fiber. The fiber was put into rigor in one of the back troughs and then transferred to the front trough for measurement of its dimensions. The length, width, and height of the fiber were measured using a compound microscope with a scale in the eyepiece. The cross-sectional area was calculated as $\pi/4 \times$ [extreme width] × [height at the center of the fiber] (Blinks, 1965; Goldman and Simmons, 1984). Two vertical masks were placed in front of the cylindrical lens to prevent the laser beam from striking the aluminum T-clips. This masking reduced sudden tension artifacts at the laser pulse (Goldman et al., 1984a). The fiber was then placed in relaxing solution again.

For experimental trials the fiber was put into rigor (with stirring) (Fig. 1), into Ca-rigor solution, and then into Ca-rigor solution with caged ATP. The fiber was immersed in each solution for 1–2 min to allow the interior of the fiber to exchange completely. Finally, the fiber was transferred to the front trough containing paraffin oil for caged ATP photolysis. Depending on the isotonic tension value selected for that trial, the fiber was stretched or released (*Release* in Fig. 1) slightly to set the rigor tension to a value slightly below the selected level. On photolysis of the caged ATP (*Flash* in Fig. 1), the active tension of the fiber was clamped at an isotonic level slightly above the rigor tension. The fiber contracted isotonically for 200–500 ms, and when the ATP available from photolysis was hydrolyzed, shortening stopped as the fiber went back into rigor at the shorter length. At ~1 min after photolysis, the fiber was released to zero tension (*Slack* in Fig. 1) to facilitate switching of the motor from isotonic back to length mode, transferred again to the relaxing solution, and then restretched to the original length. Using the same procedure, fibers were contracted and relaxed several times (3–12). The amount of ATP liberated by photolysis was varied by altering the initial concentration of caged ATP or the laser pulse energy or both (Goldman et al., 1984a).

Measurement of the concentration of photoliberated ATP

For a calibration of ATP concentration liberated by photolysis inside the fiber, caged ^{3}H-ATP was photolyzed within single fibers held isometric, and the photochemical and enzymatic reaction products were analyzed by high-pressure liquid chromatography and liquid scintillation counting. The concentration of photolyzed caged ATP was calculated from the initial amount of labeled caged ATP in the fiber, the proportion photolyzed, and the bulk concentration of caged ATP in the Ca-rigor solution. In a caged ^{3}H-ATP experiment, a ~12-mm-long fiber segment was mounted between the hooks with aluminum T-clips. The ends of the fiber extending outside

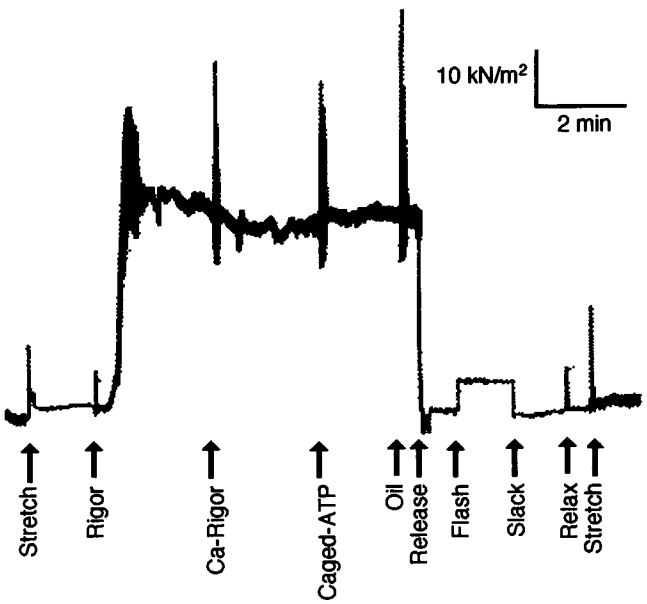

FIGURE 1 Strip chart recording of the tension from a fiber showing the protocol for isotonic contractions initiated by photolysis of caged ATP. The fiber is initially in relaxing solution. At *Stretch*, the fiber was stretched to a sarcomere length of 2.8 μm. The fiber was put into *Rigor* solution at the next arrow, and the trough was vibrated vertically to stir the contents. The stirring stopped when rigor tension was fully developed; the trace became thinner. The fiber was next placed in *Ca-rigor* solution, then into another trough with Ca-rigor + 530 μM caged ATP. At the arrow marked *Oil*, the fiber was transferred to the front trough filled with paraffin oil. At *Release* the fiber was released to decrease force to 2% of isometric active tension. The photolysis laser pulse occurred at *Flash*, and tension rose to the isotonic clamping level (5% P_o) and remained there as the fiber shortened to 2.30 μm and went back into rigor. The fiber was released to zero tension at *Slack*, and the tension clamp was switched off. The fiber was then transferred to Relaxing solution and finally restretched to 2.78 μm sarcomere length. Fiber cross-sectional area was 8163 $(\mu m)^2$; temperature was 20.4°C.

the 8-mm trough were allowed to dry in air. This arrangement minimized transfer of radioactive solution adhering to the outside of the fiber between troughs and prevented radioactive caged ATP from entering spaces within the T-clips.

The fiber was prepared for photolysis using the same solutions and procedure as described above (see Experimental procedure), except that the Ca-rigor solution contained 2–2.3 mM caged ^{3}H-ATP (loading solution). ATP was released by photolysis, and the fiber was allowed to contract isometrically in oil for 1–2 min after photolysis. The fiber was then immersed for ~4 min in a washout solution, relaxing solution with 0.2 mM unlabeled caged ATP, 0.2 mM ADP, and 0.1 mM AMP added. The fiber was immersed for 2 min each in two more aliquots of the washout solution. The three postphotolysis washes, the loading solution, paraffin oil after the photolysis, and the fiber after washing were saved for counting of radioactivity.

The Ca-rigor solution and the first washout solution were stored at −80°C until analysis. Nucleotides and caged nucleotides in the solutions were separated by using an analytical C_{18} high-pressure liquid chromatography column (Waters, Milford, MA; Partisil SAX; 10-μm pore size) and an isocratic running buffer of 75% 325 mM $NH_4H_2PO_4$, at pH 4.25, and 25% acetonitrile flowing at 3 ml/min. The elution was monitored at 254 nm. Fractions of 1 ml were collected and counted along with standards, loading solution, and the oil for 1 min in a liquid scintillation counter (model LS 7500, Beckman, Fullerton, CA) after addition of 4 ml scintillation fluid (Ecolite Plus, ICN Biochemicals, Costa Mesa, CA).

RESULTS

Determination of [ATP_u]

The concentration of ATP photoreleased into the fiber [ATP_r] was measured with radioactive caged ^{3}H-ATP. After the photolysis of caged ^{3}H-ATP, 12-mm-long fibers immersed in oil and extending beyond the solution well (see Methods section) contracted isometrically (Fig. 2). After the laser pulse, tension decreased transiently at high energy (Fig. 2 *A*) and then increased to a nearly steady value corresponding to full activation. The transient tension decrease was smaller at low energy (Fig. 2 *B*). Even though the ends of the fibers and the attachments were dried out, the tension responses to release of ATP in the 12-mm-long fibers were similar to those obtained with normal fibers 2–3 mm long (Goldman et al., 1984b) (Fig. 4 *A*).

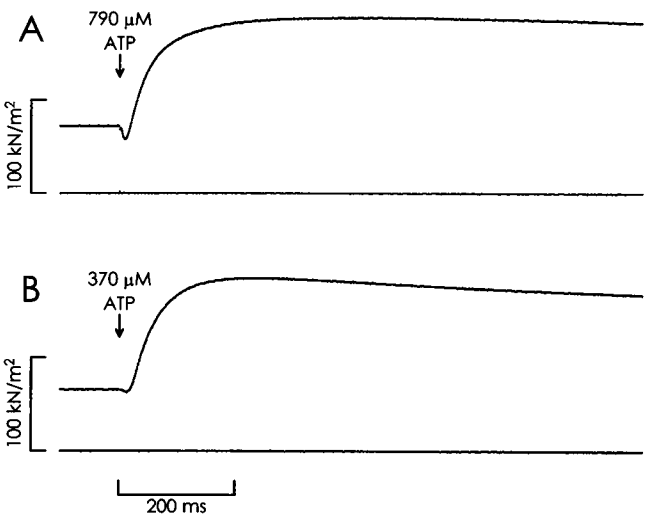

FIGURE 2 Isometric photolysis trials with a 12-mm-long fiber used for determination of the proportion of caged ATP photolyzed. The fiber was loaded with 2.5 mM caged ^{3}H-ATP and transferred to paraffin oil. (*A*) and (*B*) show transients initiated by laser pulses of 1.48 and 0.7 J/mm^2 measured at the cylindrical lens. Fiber dimensions were length, ~12 mm, 8 mm in the solution trough; sarcomere length, 2.75 μm; and cross-sectional area, 3680 (μm)^2. Temperature was 19.2°C.

The total radioactive counts washed out of the fiber divided by the specific activity of the caged ^{3}H-ATP loading solution (in counts per microliter) provide an estimate of the volume transferred to the photolysis trough and then to the washout solutions. In Fig. 3 *A*, the volume estimated from the total radioactive counts washed out of the fiber (solution space) is plotted for a series of fibers against the optically measured fiber volume. The points fall near the plotted line with slope 1.0, indicating that the volume of solution analyzed for photolysis corresponded closely to the fiber volume itself. The ratio of solution space to optically measured volume averaged 0.96 ± 0.02 (SD, n = 10). When fibers were visualized in paraffin oil using a compound microscope, the aqueous layer outside the fiber was <1 μm thick, indicating negligible carry-over of solution between troughs along the central length of the fiber. However, before we used the long fibers with dried ends extending beyond the trough, the radioactive counts exceeded those expected from the fiber volume by ~35%, indicating that a volume of solution (presumably in the T-clips) was carried over from the radioactive loading trough into the photolysis trough and the washes (Ferenczi et al., 1984). The dry-end fiber method seems to effectively eliminate this problem.

The high-pressure liquid chromatography elution profile of the radioactive nucleotides and caged ATP are shown in Fig. 3 *B*. Labeled ADP, ATP, and caged ATP are well resolved. Before the photolysis of caged ^{3}H-ATP (*filled circles*), most of the counts were in the caged ^{3}H-ATP peak, with <1% in the ^{3}H-ADP and ^{3}H-ATP peaks, indicating that the caged ^{3}H-ATP supplied by Dr. Homsher was very pure.

After photolysis, isometric contraction, and washout into relaxing medium containing carrier nucleotides (see Methods section), the elution profile of the fiber contents (Fig. 3 *B*, *open circles*) had reduced counts in the caged ^{3}H-ATP peak and correspondingly increased counts of ^{3}H-ADP. Production of ^{3}H-ADP was expected because time was allotted for the fiber to hydrolyze the ATP liberated from caged ATP. The small peak in the position of ^{3}H-ATP increased only to 1.5% of the total counts after photolysis. The ratio of counts in ^{3}H-ADP to total counts (^{3}H-ADP + ^{3}H-ATP + caged ^{3}H-ATP) after photolysis gives the proportion of caged ATP photolyzed (photochemical conversion).

In earlier experiments when AP_5A, an inhibitor of myokinase (2 ADP ⇔ ATP + AMP) activity, was not included in the experimental medium, a peak corresponding to ^{3}H-AMP appeared near the solvent front after photolysis (Ferenczi et al., 1984) amounting to ~30% of the ^{3}H-ADP peak. The

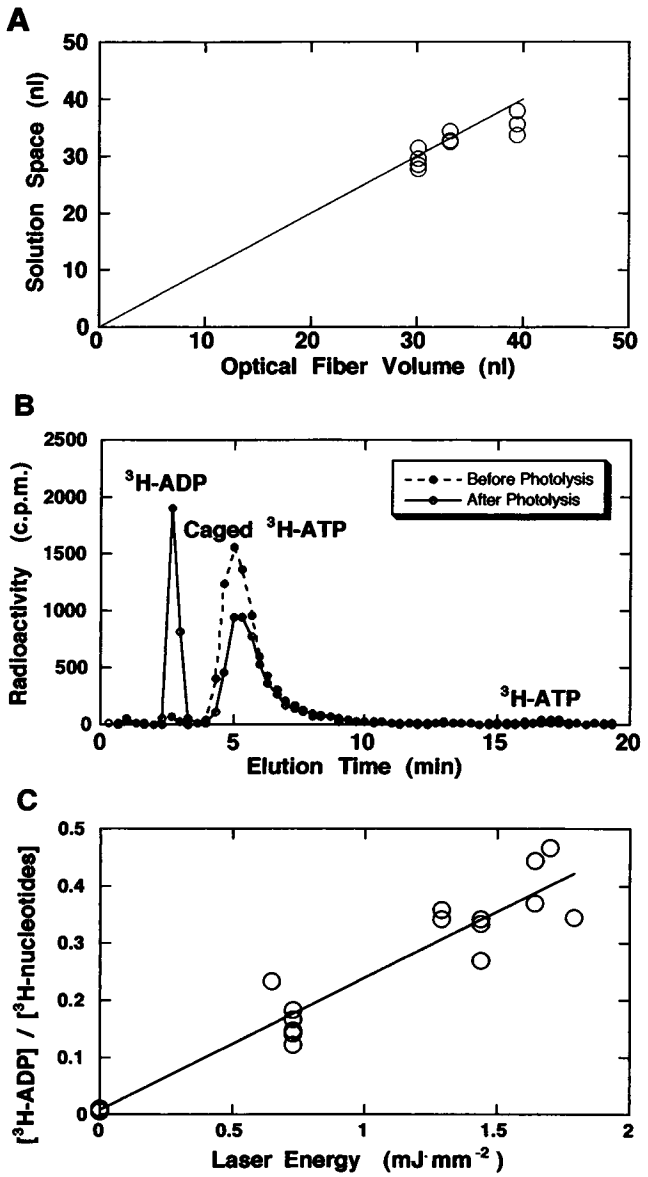

FIGURE 3 Measurement of photochemical conversion using caged ^{3}H-ATP. (*A*) Solution space according to radioactive counts washed out of fibers plotted against the volume measured optically. The line indicates equal solution space and volume. (*B*) Elution profiles of ^{3}H in the loading solution (●) and in the fiber after photolysis and 1 min of incubation to hydrolyze the photoreleased ATP (○). (*C*) Proportion of caged ATP photolyzed and then converted to ADP by enzymatic activity of the fiber vs. laser energy density measured at the cylindrical lens. The ordinate is the ratio of counts in ^{3}H-ADP to total counts of ^{3}H-nucleotides (^{3}H-ADP + ^{3}H-ATP + caged ^{3}H-ATP). The regression line represents $y = 0.232 \cdot x + 0.0075$. The correlation coefficient is $r = 0.962$.

counts near the solvent front did not change when AP_5A was present (Fig. 3 *B*).

The laser photolysis energy density was measured before the focusing optics through a rectangular slit that projected to the fiber position (see Methods section). It was important to measure the energy density from the specific region of the laser beam that illuminated the fiber because the energy density of the laser beam was not uniform. The photochemical conversion increased linearly with laser energy (Fig. 3 *C*), with slope 0.232 ± 0.027 mm^2/mJ (95% confidence limit, $n = 19$, $r = 0.962$). Therefore, $[ATP_r]$ for the sliding distance experiments was calculated as (slope) · (laser energy density) · (concentration of caged ATP in the Ca-rigor solution).

The concentration, $[ATP_u]$, of ATP utilized by actomyosin was calculated by subtracting from $[ATP_r]$ the concentration (M_H) of myosin heads in the H-zone (nonoverlap region of the A-band) at the final sarcomere length (L_f). $[M_H] = [M_o] \cdot (L_f - 2.4)/(3.8 - 2.4)$. This small correction, <45 μM, was applied if L_f was >2.4 μm because ATP binds to myosin as rapidly as to actomyosin, but under the present conditions, the hydrolysis products are not released by myosin during the <500 ms isotonic shortening period (Trentham et al., 1972).

Shortening velocity and distance

In Fig. 4 *A*, 380 μM ATP was released from caged ATP for an isometric activation and for two isotonic ones in which the tension level was clamped to 4% of isometric tension (P_o). After the photolysis of caged ATP, tension (bottom set of traces) decreased briefly and then increased to either the isometric or isotonic level. The sarcomere lengths, measured by white light diffraction, are shown as the upper set of traces. Peak shortening velocities were reached 5–20 ms after initiation of the tension clamp. Shortening velocity decreased gradually as the concentration of ATP decreased in the fiber and ADP accumulated. Finally, the shortening stopped when the ATP in the fiber was exhausted and the fiber was then in rigor at the shorter length.

The white light diffraction method used to measure shortening predominantly detects ordered sarcomeres, so potential disorder of the striations might possibly bias the measurements of sliding distance. To check this point, we measured sarcomere lengths before and after shortening by optical microscopy at four to seven positions along the fibers in paraffin oil and compared the results to the output of the white light diffraction instrument (Table 2). The dispersion of sarcomere lengths increased after shortening, but the differences between the sarcomere lengths measured directly by microscopy and by white light diffraction were not statistically significant (Table 2). Thus the diffraction method reported an unbiased average sarcomere length.

We were concerned that reflection or refraction of the photolysis light at the fiber surface might reduce ATP release in some regions of the fiber because the fiber refractive index ($n = 1.38$) is lower than that of the paraffin oil ($n = 1.47$). We tested whether the differing refractive indices affected the results by replacing the paraffin oil used in most of the experiments with very low viscosity silicone oil (200 silicone fluid, viscosity 2 centistokes, index of refraction 1.39; Dow Corning). In a comparison of 9 trials with paraffin oil and 13 with silicone oil, neither the peak velocity (slope of the sarcomere length trace) nor the extent of shortening per mol of released

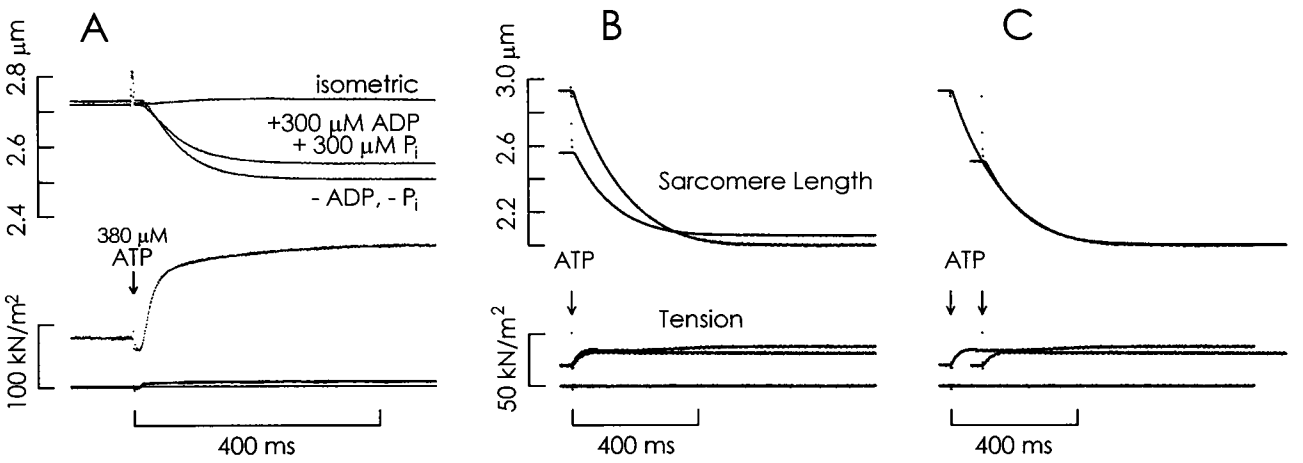

FIGURE 4 Isometric and isotonic contractions initiated by photorelease of ATP in the presence and absence of ADP and P_i. All recordings were filtered through 500-Hz notch filters to eliminate imposed sinusoidal oscillations as shown in Fig. 7. (*A*) Sarcomere length (*upper group of traces*) and tension (*lower group of traces*) were measured during an isometric contraction and isotonic contractions at 4% P_o load in the absence (−ADP, $-P_i$) or presence of 300 μM ADP and 300 μM P_i in the photolysis solution. The isotonic tension traces superimpose. The lowest line is the relaxed baseline at sarcomere length 2.7 μm. Fiber length: 2.3 mm; cross-sectional area, 3430 $(\mu m)^2$. Temperature was 19.1°C. (*B*) Comparison of shortening from high [ATP] with shortening from low [ATP] plus added ADP and P_i. A fiber shortened isotonically starting at a sarcomere length of 2.93 μm after release of 826 μM [ATP] and from 2.56 μm starting at 554 μM [ATP] in the presence of 300 μM ADP and 300 μM P_i. The lowest line is the relaxed baseline. (*C*) The recordings of (*B*) were shifted to superimpose the low and high [ATP] traces. Fiber length: 2.11 mm; cross-sectional area, 2360 $(\mu m)^2$. Temperature was 20.2°C.

ATP were significantly different. Thus nonuniform ATP release attributable to reflection and refraction at the fiber surface is not an appreciable problem.

The peak velocity of shortening 5–20 ms after initiation of the tension clamp increased when $[ATP_u]$ was increased (compare Figs. 4 and 7 *A*) and velocity gradually saturated at high $[ATP_u]$ (Fig. 5). The velocity and total shortening distance decreased as the isotonic load was increased (Figs. 5 and 7). The velocity, V, was analyzed by using a modified Michaelis-Menten equation of the form $(V = V_s \cdot ([ATP] - [M_o])/\{([ATP] - [M_o]) + K_m\})$, where V_s is velocity at a saturating concentration of MgATP, K_m is the MgATP concentration at half saturation velocity, and $[M_o] = 154$ μM. In this analysis, initial [MgATP] was approximated by $[ATP_u] - [M_o]$ at $[ATP_u] > [M_o]$ because myosin heads bind the photoreleased ATP quickly and with high affinity. The curves in Fig. 5 represent fitted hyperbolic relations for $[ATP_u] > 230$ μM. The data show that shortening velocity saturates at lower ATP concentrations when the load is higher. At isotonic tension levels near 0.06 P_o, V_s was estimated according to the fitted curve at 4.8 $\mu m \cdot s^{-1}$ per half sarcomere, and K_m was 364 μM.

At 3 mM MgATP, velocity of shortening at zero load was found to be 6.8 ± 0.9 $\mu m \cdot s^{-1}$ (mean ± SE, $n = 5$) by the slack test, somewhat higher than the 4.8 $\mu m \cdot s^{-1}$ saturating value estimated from the curve in Fig. 5 *A* and much higher than the 2.7 $\mu m \cdot s^{-1}$ value directly observed in our caged ATP photolysis experiments at $[ATP_u] \leq 800$ μM. The lower velocity at 800 μM $[ATP_u]$ suggests that rigor cross-bridges, nucleotide-free or with ADP or caged ATP bound, cause a substantial internal load.

Release of >800 μM ATP at low load or >1200 μM ATP at higher load caused excessive shortening of the fibers into the sarcomere length region (≤2.0 μm) where the thin filaments crossed the M line. For this reason, in D_i experiments $[ATP_u]$ was limited to values leading to ≤400 nm of filament sliding. Shortening distance, D_s, per half sarcomere was taken as half the decrease in sarcomere length from the

TABLE 2 Sarcomere lengths determined by microscopy and the diffraction method

			Before photolysis			After photolysis		
Experiment	$[ATP_u]$ (μM)	Tension (% P_o)	LM (μm)	LL (μm)	LM-LL (μm)	LM (μm)	LL (μm)	LM-LL (μm)
1	777	14	2.73 ± 0.06	2.78	−0.05	2.04 ± 0.09	2.06	−0.02
2	772	15	2.85 ± 0.06	2.88	−0.03	2.08 ± 0.06	2.04	0.04
3	590	10	2.83 ± 0.05	2.81	0.02	2.20 ± 0.08	2.26	−0.06
4	581	12	2.70 ± 0.07	2.62	0.08	2.31 ± 0.09	2.23	0.08
5	544	8	2.84 ± 0.07	2.81	0.03	2.25 ± 0.08	2.33	−0.06
	Average ± SD				0.01 ± 0.05			−0.01 ± 0.06

Abbreviations: LM, sarcomere length measured by microscopy at four to seven positions along the fiber; LL, sarcomere length measured by the white light diffraction method; and LM-LL: difference between LM and LL.

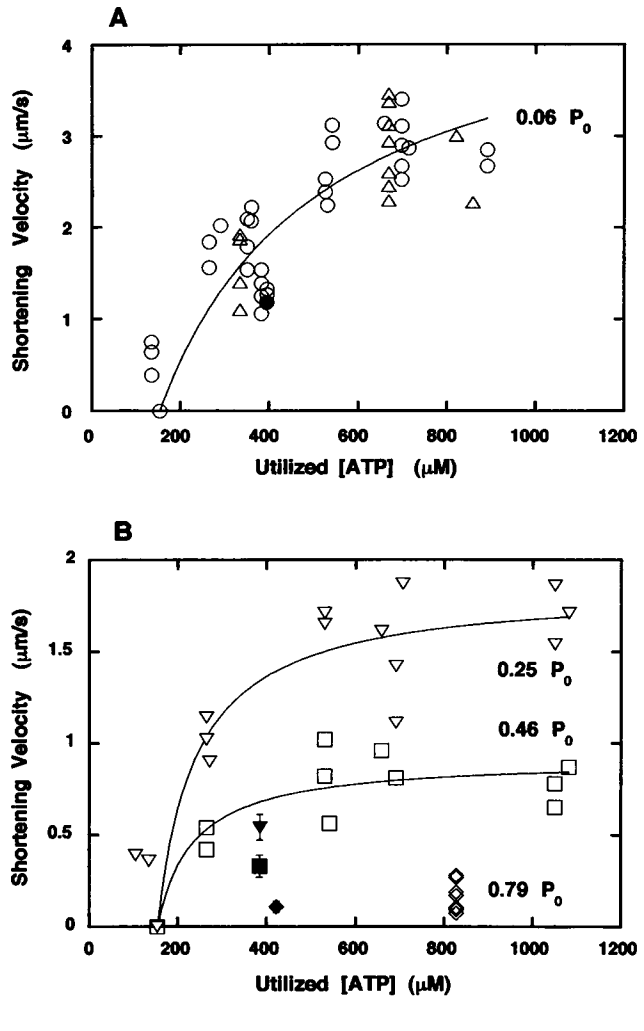

FIGURE 5 Peak shortening velocity after photoliberation of various amounts of ATP. The velocity in each trial was measured at 5–20 ms after initiation of the tension clamp. (*A*) The load was ~0.06 P_o. For circles, 500-Hz sinusoidal length changes at amplitude of 1–4 nm/sarcomere peak-to-peak were applied. For triangles, no sinusoidal length change was used. (*B*) The load was 0.25 (▽), 0.46 (□), or 0.79 (◇) of P_o. For the open symbols, ADP or P_i were not added to the photolysis solution. For closed symbols, 300 μM ADP and 300 μM P_i were added to the photolysis solution. The error bars indicate mean ± SE for four to six values. The initial concentration of caged ATP was 0.45–3.88 mM, and laser pulse energy was varied between 1.08 and 1.7 mJ/mm^2. [ATP] was calculated from the calibration data in Fig. 3, as explained in the text. The solid lines indicate modified Michaelis-Menten curves ($V = V_s \cdot ([ATP] - [M_o])/\{([ATP] - [M_o]) + K_m\}$) fitted to the data. The velocity, V_s, at saturating [ATP] and K_m were 4.83 μm · s^{-1}, and 364 μM at 0.06 P_o; 1.84 μm · s^{-1} and 84 μM at 0.25 P_o; and 0.91 μm · s^{-1} and 79 μM at 0.45 P_o.

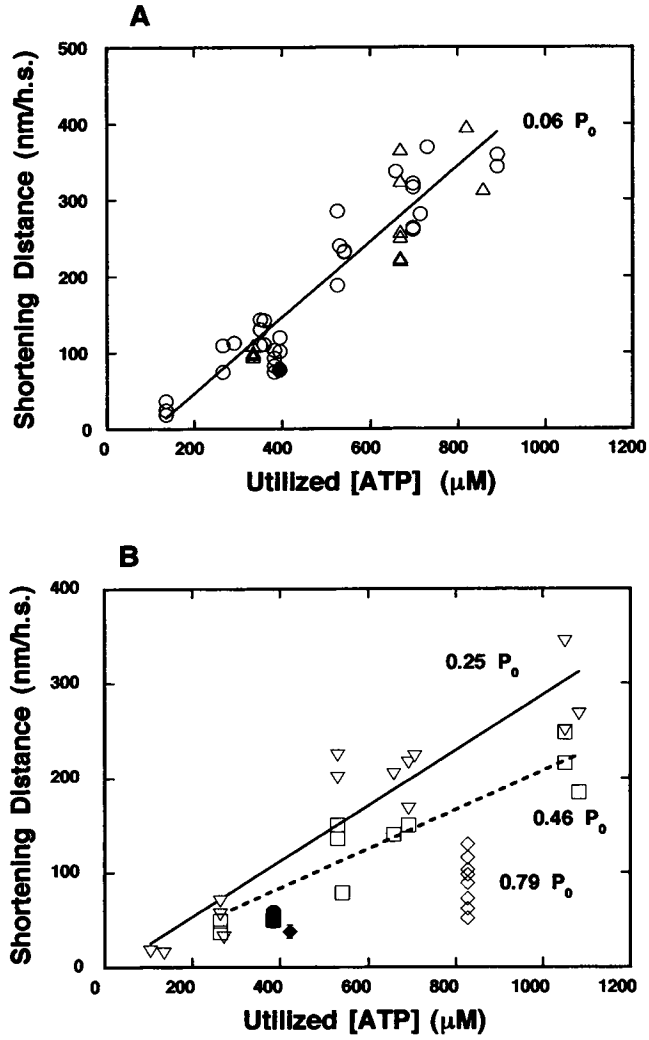

FIGURE 6 Shortening distance during isotonic contraction vs. utilized [ATP]. Shortening distance was measured as the difference between the half-sarcomere lengths before and after the shortening. The symbols and conditions are the same as those in Fig. 6. The straight lines are regression lines to the data at 0.06, 0.25, and 0.46 P_o in the absence of ADP and P_i.

initial to the final rigor states. D_s increased almost linearly with [ATP_u] and decreased as the isotonic tension was increased (Fig. 6).

Effect of ADP and orthophosphate (P_i)

As the fiber shortened, hydrolysis of ATP by actomyosin caused the ATP concentration in the fiber to fall from its initial value to zero, and concomitantly, the ADP concentration increased. Inasmuch as external loads decrease velocity and D_s, it seemed likely that the internal load of nucleotide-free or ADP-bound cross-bridges would also limit velocity and D_s, especially toward the end of the shortening phase. This was tested by photolyzing smaller amounts of ATP and adding ADP and P_i to the photolysis solution. In Fig. 4 *A*, shortening traces are compared in trials in which 380 μM ATP was released in the absence and presence of an initial 300 μM ADP and 300 μM P_i. Adding ADP and P_i to the photolysis medium reduced D_s ~20% in this experiment. At all four relative loads shown in Fig. 6, adding ADP and P_i at low [ATP_u] (*closed symbols*) reduced D_s.

Low ATP release with added ADP and P_i simulates the biochemical condition in the fiber during the latter half of shortening starting from high [ATP]. Combined data from

high-[ATP] and low-[ATP] + ADP + P_i trials are used later to correct for the drag of nucleotide-free and ADP-bound cross-bridges, assuming that a low-[ATP] + ADP + P_i trial mimics the latter half of a high-ATP trial. We tested this assumption by experiments of the type shown in Fig. 4, *B* and *C*. A fiber was shortened isotonically starting at 2.93 μm sarcomere length by release of 826 μM ATP. The fiber length was decreased in relaxing solution and then contracted from rigor at 2.56 μm by photoreleasing 554 μM ATP in the presence of 300 μM ADP and 300 μM P_i. As expected, less shortening occurred for the smaller amount of ATP released (Fig. 4 *B*). In Fig. 4 *C*, the same data are shown, but the sarcomere length trace from the low-[ATP] trial has been shifted to superimpose it on the latter phase of the high-[ATP] trial. The shapes of the two traces are very similar, indicating that the conditions of the low-[ATP] + ADP + P_i trial do approximate those in the fiber during the final phase of shortening after release of high [ATP].

Stiffness

We measured the stiffness of the fiber during shortening to estimate the proportion of myosin heads interacting with the actin filament during sliding. The stiffness was measured by detecting the sinusoidal tension and sarcomere length oscillations (Fig. 7) caused by an applied 500 Hz sinusoidal length change, 1–4 nm per sarcomere peak-to-peak. Experiments without length oscillations showed that the sinusoidal length changes did not affect shortening velocity or shortening distance (compare *circles and triangles* in Figs. 5 *A* and 6 *A*). In stiffness experiments, the sarcomere length and tension signals were filtered through 500 Hz, Q = 2, recursive, digital band-pass filters to extract the sinusoidal components and to reduce noise (Fig. 7, *lower traces*).

The stiffness (S_{obs}) was calculated as the amplitude ratio of the tension and sarcomere length oscillations relative to the ratio in rigor before photolysis. To correct for the effect on rigor stiffness attributable to incomplete overlap between the thick and thin filaments at the initial (stretched) length, stiffness (S_r) relative to that in rigor at full overlap was calculated as $S_r = S_{obs} \cdot (3.8 - L_i)/(3.8 - 2.4)$, where the L_i is initial sarcomere length in μm. This correction assumes that rigor stiffness decreases linearly with sarcomere length between 2.4 and 3.8 μm (Tawada and Kimura, 1984).

S_r decreased to about half its initial value just after a laser pulse (Fig. 8 *A*). During the initial period of shortening, the stiffness was lower at lower loads. Then the stiffness increased gradually as [ATP] decreased and filament overlap increased. In the final rigor state after shortening, stiffness was slightly less than the initial value, probably because the sarcomeres became somewhat disordered during the isotonic period (Table 2). The intensity of light diffraction by the sarcomeres was typically decreased at the end of each trial, consistent with some disorder.

The variation of S_r with load is rather small in Fig. 8 *A* because at a given instant after the laser pulse the fibers had shortened more at the lower loads, and the resulting increased filament overlap partly compensated for the reduced

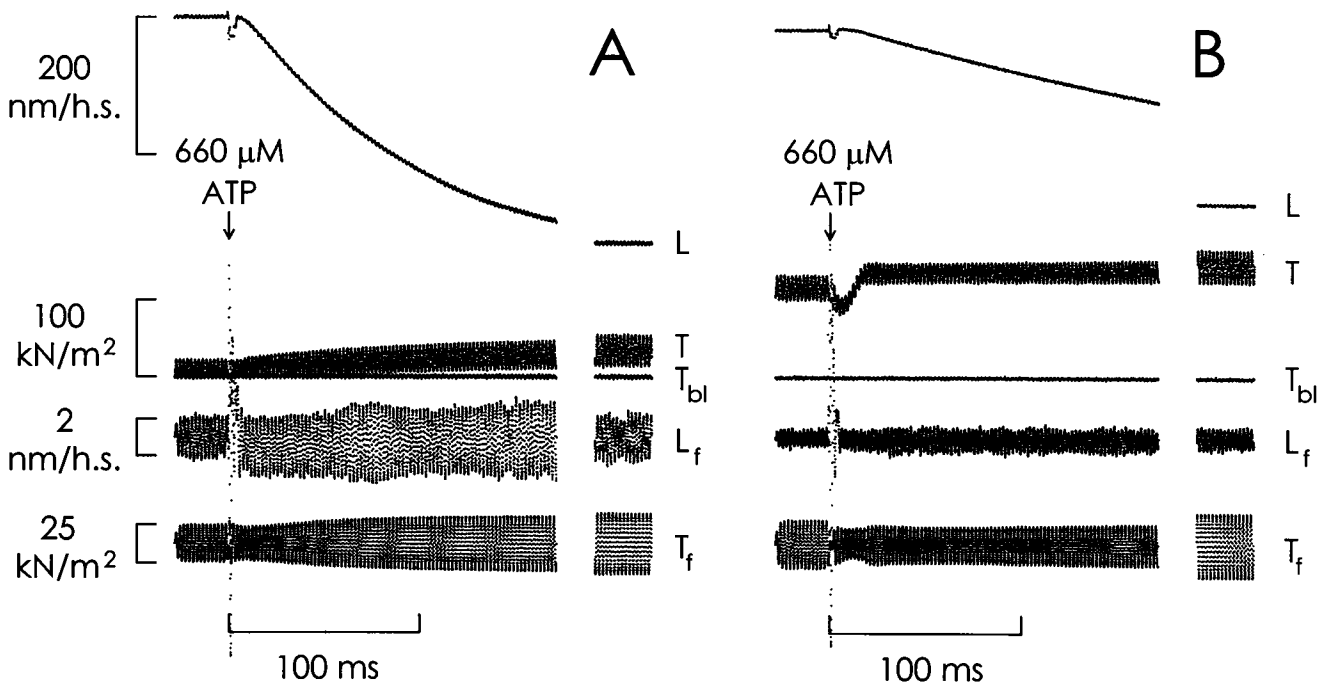

FIGURE 7 Stiffness measurements during isotonic shortening. Sarcomere length was oscillated sinusoidally at 500 Hz. Steady sarcomere length (L) and tension (T) levels at ~10 s after photolysis are shown as the short recordings to the right of each panel. The lower sarcomere (L_f) and tension (T_f) traces were obtained by filtering the original signals through 500-Hz digital band-pass filters. (*A*) Isotonic tension was 0.07 P_o; (*B*) isotonic tension was 0.25 P_o. Released [ATP] was 660 μM. Fiber dimensions: sarcomere length, 2.88 μm; length, 2.28 mm; cross-sectional area, 5310 $(\mu m)^2$. Temperature was 20.6°C.

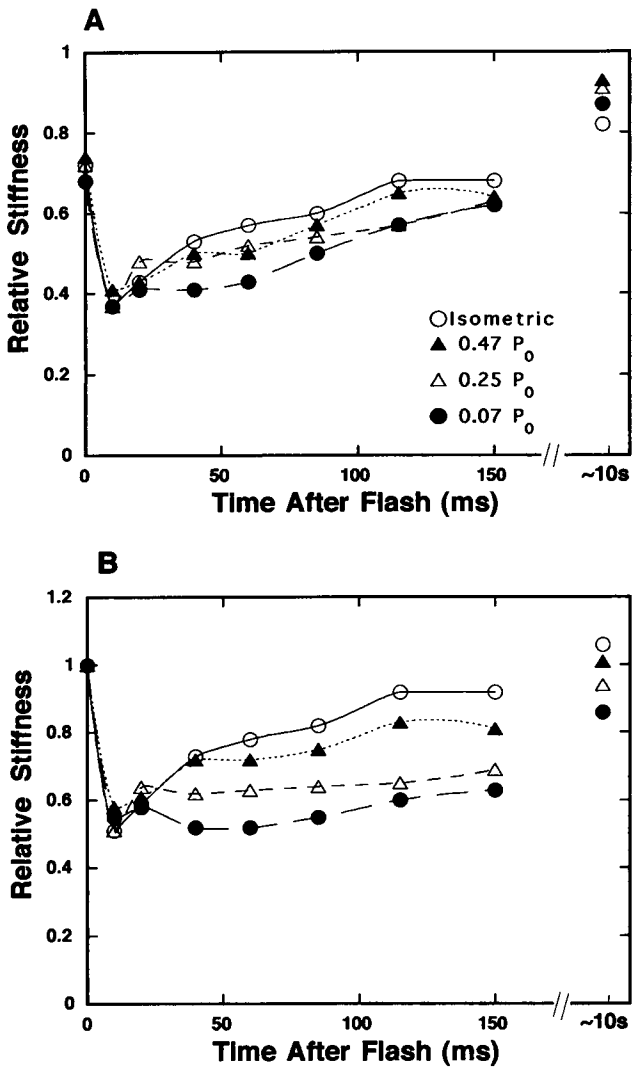

FIGURE 8 Relative stiffness change after photogeneration of ATP; 530–713 μM ATP was photogenerated at time 0. Isometric contraction (○); isotonic contraction at 0.07 P_o (●); 0.25 P_o (△); 0.47 P_o (▲). Each plotted point shows the mean of four to eight measurements. (*A*) Stiffness (S_r) relative to rigor stiffness at full overlap; (*B*) stiffness (S_{over}) relative to rigor stiffness estimated at each sarcomere length during shortening. S_{over} depends on load more than S_r.

stiffness. This can be shown by correcting for the filament overlap at each time, as follows. Assuming that stiffness is proportional to the number of myosin heads attached to actin, the ratio (S_{over}) of attached myosin heads to total heads in overlap zone is given by $S_{obs} \cdot (3.8 - L_i)/(3.8 - L)$, where L is the sarcomere length at the time of measurement (Fig. 8 *B*). During the initial period of shortening (e.g., at 50 ms after the laser pulse), the variation of S_{over} (Fig. 8 *B*) with load is larger than that of S_r (Fig. 8 *A*) because the effect of filament overlap on stiffness is taken into account. The stiffness (S_{over}) in the initial (high speed) period of shortening was ~0.5, 0.6, 0.7, and 0.8 of the full overlap rigor stiffness at 0.07, 0.25, 0.45, and 1.0 P_o, respectively. Stiffness (both S_r and S_{over}) gradually increased and finally reached ~1 at the end of shortening.

The stiffness value to be used in calculating D_i by Eq. 1 must account for the proportion of the sliding obtained with each value of stiffness. Thus the average (S_a) should be weighted according to the velocity (V):

$$S_a = \frac{\int_0^{t_f} S_r V\,dt}{\int_0^{t_f} V\,dt} = \frac{\int_{L_i}^{L_f} S_r\,dL}{(L_f - L_i)} \qquad (2)$$

where t_f is the duration of the recording after the laser pulse and L_i and L_f are the initial and final sarcomere lengths. As Eq. 2 shows, a velocity-weighted time average corresponds to a "distance average." Assuming again that stiffness is proportional to the number of myosin heads attached to actin at each instant, S_a gives the average proportion of heads attached during shortening relative to the total number at full overlap.

The integral on the right side of Eq. 2 was approximated as the sum of $S_r \cdot \Delta L$ for the seven discrete time intervals plotted in Fig. 8 *A* (excluding the initial and final rigor points), where ΔL is the corresponding amount of sarcomere shortening. The values obtained for S_a are summarized in Table 3 in various conditions. S_a was almost independent of isotonic tension because at low tension, increased filament overlap caused by an increased amount of shortening offset the lower S_{over} values. The addition of ADP and P_i increased S_a at each isotonic tension (Table 3).

Interaction distance

If the shortening distance, D_s, multiplied by average stiffness, S_a, is plotted vs. the concentration of ATP utilized ($[ATP_u]$) (Fig. 9 *A*), the slope of the plot ($D_s \cdot S_a/[ATP_u]$) multiplied by the total concentration $[M_o]$ of myosin heads gives the interaction distance, D_i (see Eq. 1). The squares in Fig. 9 *B* show D_i calculated this way for the data in trials starting at 700–800 μM ATP. The diamonds (*lowest curve*) in Fig. 9 *B* show D_i calculated for trials with 350 μM ATP + 300 μM ADP + 300 μM P_i. In the latter case, the drag of nucleotide-free cross-bridges and ones with ADP bound reduced D_i at relative loads below 0.8.

We could partly correct for the drag of rigor cross-bridges by calculating D_i during the initial period of shortening, as [ATP] decreased from 700–800 μM to ~350 μM and [ADP] and $[P_i]$ increased to ~350 μM. D_i during this period is given by the slopes of the right-hand set of lines in Fig. 9 *A* multiplied by $[M_o]$. These higher slopes correspond to $\{(D_s \cdot S_a)_{high} - (D_s \cdot S_a)_{low}\}/\{[ATP_u]_{high} - [ATP_u]_{low}\}$ where the "high" and "low" subscripts refer to the starting [ATP]. The D_i values obtained for the initial shortening are plotted as circles in Fig. 9 *B*, extending up to 60 nm at 0.07 P_o relative load. This procedure is justified by the finding (Fig. 4 *C*) that shortening after reduced ATP liberation in the presence of ADP and P_i simulates the final period of

TABLE 3 Summary of numerical data

$[ATP_u]$ (μM)	$[ADP]_{initial}$ (μM)	Tension (% P_o)	S_a	$V_{initial}$ ($\mu m \cdot s^{-1}$)	n	D_i (nm)
688 ± 40	0	7.2 ± 0.6	0.59 ± 0.04	2.70 ± 0.09	12	60
336 ± 15	0	6.3 ± 0.8	0.62 ± 0.05	1.64 ± 0.10	13	29
370 ± 2	300	4.1 ± 1.6	0.67 ± 0.04	1.18 ± 0.10	5	22
807 ± 89	0	24.5 ± 1.3	0.65 ± 0.06	1.60 ± 0.06	8	40
363 ± 3	300	26.3 ± 1.4	0.69 ± 0.03	0.54 ± 0.06	5	18
791 ± 116	0	45.8 ± 2.3	0.61 ± 0.06	0.78 ± 0.06	7	23
362 ± 5	300	45.7 ± 3.3	0.72 ± 0.05	0.33 ± 0.06	4	16
808 ± 4	0	77.6 ± 2.8	0.63 ± 0.05	0.16 ± 0.06	6	11
397 ± 4	300	80.6 ± 2.8	0.68 ± 0.04	0.11 ± 0.06	6	10

$[ATP_u]$ = concentration of ATP utilized by actomyosin = ATP liberated from caged ATP − concentration of myosin heads in the H-zone; see Methods section. $[ADP]_{initial}$ = concentration of ADP and P_i added to the photolysis solution. Tension = isotonic force relative the isometric value. S_a = average stiffness of the fiber during sliding relative to that in rigor at full overlap between the thick and thin filaments. $V_{initial}$ = peak shortening velocity measured 5–20 ms after the photolysis pulse. n = number of fibers. D_i = at each relative load, interaction distance calculated for upper or lower range of $[ATP_u]$ values. For the upper range, $D_i = [M_o] \cdot \{(D_s \cdot S_a)_{high} - (D_s \cdot S_a)_{low}\}/\{[ATP_u]_{high} - [ATP_u]_{low}\}$. For the lower $[ATP_u]$ range, $D_i = [M_o] \cdot (D_s \cdot S_a)_{low}/[ATP_u]_{low}$.

shortening after release of a high [ATP]. The higher slopes of the lines in Fig. 9 *A* between ~800 μM and ~400 μM $[ATP_u]$ compared with the slopes between ~400 μM and zero $[ATP_u]$ indicate that low [ATP] and accumulating ADP decrease interaction distance. Also, the dependence of D_i on relative load (Fig. 9 *B*) is much steeper for the high $[ATP_u]$ range (*circles*) than at low $[ATP_u]$ (*diamonds*). This reduction of D_i by rigor cross-bridges (both AM and AM.ADP) results from wasting of energy, as can be shown by an efficiency calculation given in the Discussion section. Thus the interaction distance during the initial period of shortening (*circles* in Fig. 9 *B*) was higher than for individual traces (*lower curves*) because there was less drag from nucleotide or ADP-bound cross-bridges during the first part of shortening at high ATP. However, drag of nucleotide-free cross-bridges is probably not completely eliminated during the initial period because the velocity of shortening was not saturated at 700–800 μM ATP (Fig. 5). The estimated values of D_i are listed in Table 3. D_i was near 10 nm for loads near 0.8 P_o and increased up to 60 nm as the load decreased to 0.07 P_o.

DISCUSSION

By comparing the isotonic shortening obtained after release of 700–800 μM ATP with that after the release of ~350 μM ATP in the presence of 300 μM ADP and 300 μM P_i, we obtained the distance of filament sliding while myosin and actin are interacting (contributing to stiffness) per ATP molecule used by a myosin head. This interaction distance (D_i) corresponds to the sliding as [ATP] declines from 800 to 350 μM. D_i depends strongly on filament sliding velocity, increasing from 10 nm at low velocity (high load) up to at least 60 nm at high velocity (low load). Because the axial spacing between actin monomers in the thin filament is 5.5 nm (Hanson and Lowy, 1963) and the myosin head is 16–19 nm long (Elliott and Offer, 1978; Rayment et al., 1993), the ≥60 nm D_i suggests that multiple interactions between actin and myosin take place within an ATPase cycle. We consider below what types of actomyosin interactions contribute to this total D_i and what the value of D_i might be at higher [ATP]. First we consider some potential artifacts and uncertainties in determining the parameters, $[ATP_u]$, D_s, S_a, and $[M_o]$, required in order to estimate D_i.

Determination of $[ATP_u]$

We used tritiated caged ATP to measure $[ATP_u]$ because the total amount of ATP hydrolyzed within the 40-nl volume of a fiber in an experimental trial was typically only ~20 pmol. The resolution of the caged ^{3}H-ATP method was better than 0.02 pmol, adequate for the present experiments. Several possible artifacts of the method should be considered. To avoid a potential problem of unphotolyzed ^{3}H-ATP within the attachment T-clips in the calibration, long (12 mm) fibers were used so that the T-clips extended beyond the ends of the solution trough. These long fibers contracted normally, as shown in Fig. 2, and after contraction most (96%) of the ^{3}H-ATP photoreleased in the fibers was found to be hydrolyzed to ^{3}H-ADP, as expected (Fig. 3 *B*). Less than 1 μm thickness of solution was carried on the fiber surface from the caged ATP loading trough into the paraffin oil. Also, the apparent solution space given by the total radioactivity loaded into the fiber compared closely with the volume measured by using an optical microscope (Fig. 3 *A*).

Enzymatic activities other than actomyosin might contribute to ATP hydrolysis. Myokinase activity, catalyzing the reaction {2 ADP ⇔ ATP + AMP}, was detected in early experiments, but inclusion of 40 μM of the myokinase inhibitor, AP_5A, in the medium suppressed it (Fig. 3 *B*). Without creatine phosphate in the photolysis medium, creatine kinase activity was not significant. To remove residual membrane ATPases, the skinned fibers were treated with Triton X-100.

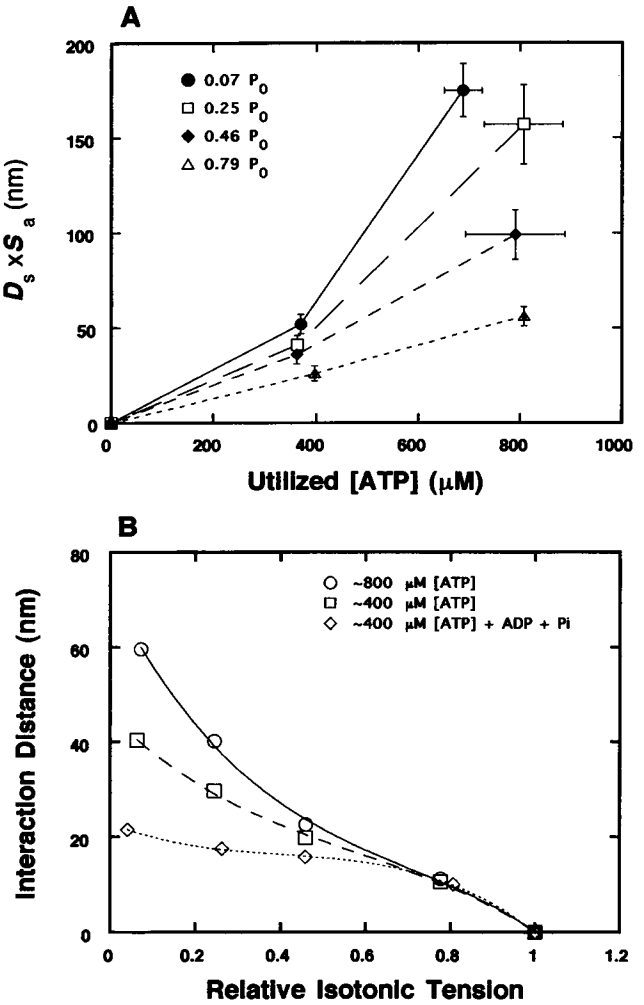

FIGURE 9 Interaction distance estimated from shortening distance (D_s), average stiffness (S_a), and [ATP] utilized. (*A*) $D_s \cdot S_a$ plotted against utilized [ATP]. Relative tension values: 0.07 P_o (●), 0.25 P_o (□), 0.46 P_o (◆), 0.79 P_o (△). Error bars, mean ± SE with 4 to 13 values. At low [ATP] (350–400 μM), 300 μM ADP and 300 μM P_i were added to Ca-rigor solution with caged ATP. (*B*) Interaction distance was estimated from the slopes of the lines plotted in (*A*) multiplied by the concentration of myosin heads (154 μM). Symbols: distance estimated from the slopes at lower [ATP] between ~400 μM and 0 (◇); average distance between ~800 μM and 0 [ATP] (□); distance estimated from the slopes at higher [ATP] between ~800 and ~400 μM (○).

If caged ATP could bind to internal constituents of the fibers, its concentration within the fiber would be higher than in the external medium. However, the relation between $[ATP_u]$ and the sliding distance was the same when $[ATP_u]$ was varied by changing either the concentration of caged ATP or the laser energy density, suggesting that binding of caged ATP within the fibers was not substantial. A direct comparison of fiber-shortening velocity in the presence and absence of caged ATP also indicated weak binding of caged ATP to actomyosin (inhibition constant for shortening velocity, $K_I \approx 1.5$ mM) (Thirlwell et al., 1995; Higuchi, Goldman and D.R. Trentham, unpublished results).

The utilized $[ATP_u]$ was determined from a calibration experiment to determine the ratio (R) of photoliberated ^{3}H-ATP to the initial concentration of caged ^{3}H-ATP as a function of the laser energy density. In principal, R should be given by a curve of the form $R = Q(1\text{-}e^{-kE})$, where Q is the photochemical conversion at infinite energy, k is a constant, and E is the laser energy density. In the low energy range used in these experiments, the deviation of this curve from linearity would be less than 5% and was therefore ignored.

Sliding distance (D_s)

D_s was measured by a white light diffraction method that avoids Bragg-angle artifacts found with laser light (Rüdel and Zite-Ferenczy 1979; Goldman, 1987b). For the present experiments, we carefully checked the calibration of the sarcomere-length instrument against microscopic measurements of striation spacing (Table 2). Uncertainty in an individual measurement of D_s was less than the inhomogeneity of sarcomere lengths within a fiber.

Proportion of myosin heads attached during sliding (S_a)

For a given interaction distance, total sliding would be lowest if the cross-bridges all act simultaneously, higher if they are asynchronous, and highest if they act sequentially. Therefore, estimation of D_i depends on knowledge of the proportion of heads attached during the sliding. We estimated this fraction from the stiffness of the fiber during sliding relative to stiffness in rigor at full filament overlap, assumed to represent the attachment of virtually all the cross-bridges (Cooke and Franks, 1980; Thomas and Cooke, 1980; Lovell et al., 1981). Stiffness relative to rigor decreased quickly to half its initial value after photolysis (Fig. 8), indicating detachment of myosin heads (Goldman et al., 1984b), and then increased gradually as the [ATP] decreased and [ADP] increased within the fiber. Stiffness during shortening was reduced as the load decreased, as expected (Ford et al., 1985). Compared with that in active isometric contraction, the stiffness at early times (~50 ms after photolysis) was ~70% during shortening at low load (0.07 P_o). This value was higher than the stiffness ratio (~40%) obtained with intact frog fibers at high velocity (Ford et al., 1985; Griffiths et al., 1993), presumably because of the relatively low concentration of ATP here.

The assumption that the stiffness indicates the proportion of cross-bridges attached to actin was made on the basis of the results of A. F. Huxley and Simmons (1973) and Ford et al. (1981), which showed that at long sarcomere lengths the stiffness during isometric contraction scales with the length of overlap region between the thin and thick filaments. However, several recent results have suggested that a substantial proportion of sarcomere compliance resides in the filaments (Kojima et al., 1994; H. E. Huxley et al., 1994;

Wakabayashi et al., 1994; Higuchi et al., 1995). If half the sarcomere compliance in rigor is attributable to thin filament extensibility (Higuchi et al., 1995), then 59–72% active stiffness during shortening (Fig. 8) relative to rigor stiffness indicates that 42–56% of the cross-bridges are attached. In this case, D_i values would be reduced to 71–78% of the results shown in Fig. 9.

The interpretation of the stiffness signal also depends on where in the myosin molecule the mechanically compliant component is located. If all of the cross-bridge compliance is within the S-1 head, then the measured stiffness is proportional to the number of heads attached, and the D_i values (e.g., Fig. 9) are representative of individual myosin head interactions with the thin filament. On the other hand, if the cross-bridge elasticity resides solely in the S-2 linkage, then single- or double-headed cross-bridge attachments would contribute the same increment of stiffness. Then the interpretation depends on whether the two heads of a given molecule are synchronized. If the two heads interact with actin independently and randomly, then 59–72% of active stiffness (representing single- and double-headed attachments) during shortening (Fig. 8) relative to rigor indicates that 36–47% of the individual myosin heads are attached. In this case, D_i values would be reduced to 61–65% of the results shown. The most extreme case is if both heads attach in rigor, but only single-headed attachments occur during active contractions. Then (still assuming elasticity all in S-2), the D_i values in Fig. 9 should be halved. At least some of the cross-bridge elasticity seems to reside within S-1 (Craig et al., 1980; Rayment et al., 1993; Irving et al., 1995), so the last case seems unlikely.

All the factors listed so far tend to reduce the proportion of cross-bridges attached (and D_i) for a given measured stiffness. A final factor that would raise the proportion is the different frequency response of active vs. rigor cross-bridges. The 500-Hz oscillation frequency used here for stiffness measurements is too low to detect the entire active cross-bridge population. Stiffness measured during active contraction is reduced to $[1/\sqrt{1/(2\pi f\tau)^2 + 1}]$ of its high frequency value, where f is frequency of oscillation (500 Hz) and τ is the time constant of tension recovery after a quick length change. Taking τ as 0.5 ms, stiffness measured at 500 Hz is reduced to 84% of the saturating value at high frequency. Thus, taking the frequency response into consideration increases D_i values by ~19%, partially compensating for the effects of filament compliance and single- vs. double-headed attachments.

Concentration of myosin heads within skinned fibers (M_o)

Total concentration of myosin heads in a fiber was taken as 154 μM (Ferenczi et al., 1984), which was estimated from the protein mass-to-volume ratio of fibers and the myosin content of 0.83 μmol/g protein found by Yates and Greaser (1983) in myofibrils. This content of myosin implies a value of 2.5 myosin molecules per 14.3 nm repeat on the thick filament. The thick filament is organized as a three-stranded structure (Maw and Rowe, 1980; Kensler and Stewart, 1983), suggesting three myosin molecules per 14.3 nm repeat and raising the estimate of $[M_o]$ to 185 μM. Marston and Tregear (1972) estimated $[M_o]$ as 240 μM from the amount of ADP binding to muscle fibers. Because interaction distance (D_i) is proportional to $[M_o]$ (Eq. 1), these alternative values would increase D_i by ~20–56%. Taking all the factors that introduce uncertainty into the calculation of D_i, the values might be larger by up to 56% or smaller by up to 39%, but the parameters we consider the most reliable have been used to calculate the D_i values given in Fig. 9 *B* and Table 3.

Efficiency of energy transduction

The efficiency (E) is given by the ratio of mechanical work to the energy liberated by hydrolysis of ATP. In isotonic conditions, the mechanical work done (W) is given by $W = P \cdot (L_i - L_f)$, where P = force and L_i and L_f = initial and final fiber lengths. The free energy liberated per mol of ATP hydrolysis is $\Delta G = \Delta G_o - RT \ln([ADP] \cdot [P_i]/[ATP])$, where ΔG_o = the standard free energy of ATP hydrolysis (30 kJ/mol) and RT = 2.5 kJ/mol. The total free energy liberated during a contraction is

$$\begin{aligned}\Delta G_T &= \int_{[ATP]_i}^{[ATP]_f} \Delta G \, d[ATP] \\ &= \Delta G_o[ATP]_f + RT\{[ADP]_f(\ln([ADP]_f) - 1) \\ &+ [P_i]_f(\ln([P_i]_f) - 1) + [ATP]_f(\ln([ATP]_f) - 1)\} \\ &- \Delta G_o[ATP]_i - RT\{[ADP]_i(\ln([ADP]_i) - 1) \\ &+ [P_i]_i(\ln([P_i]_i - 1) + [ATP]_i(\ln([ATP]_i) - 1)\}\end{aligned} \quad (3)$$

where ΔG_T = total energy liberated and subscripts "i" and "f" indicate initial and final concentrations. Efficiency is given as $E = W/\Delta G_T$. For example, between 791 and 362 μM ATP at load 0.46 P_o, the fibers shortened 115 nm per half sarcomere or 0.0827 of the initial length (115 nm/1390 nm initial half-sarcomere length). The work done per m^3 of fiber volume was $W = 0.46 \cdot 200$ kN $\cdot$ 0.0827 m = 7.58 kJ. Assuming $[ADP]_i = [P_i]_i = 2$ μM (0.1% of the initial caged [ATP]), ΔG_T is calculated from the formula above to be 21.4 J/l = 21.4 kJ/m^3. The efficiency is then E = 7.58/21.4 = 0.35. Note that the stiffness (S_a) and myosin head concentration ($[M_o]$), required to calculate D_i, do not enter into calculating the efficiency.

The efficiency for shortening between ~800 and ~400 μM [ATP] is maximal at 0.46 P_o load (Fig. 10, *upper curve*). For shortening from 400 μM [ATP] + 300 μM [ADP] + 300 μM [P_i] to exhaustion of the substrate (*lower curve*), the efficiency is considerably less. For this latter calculation, the $[ADP]_f$ and $[P_i]_f$ were assumed to equal

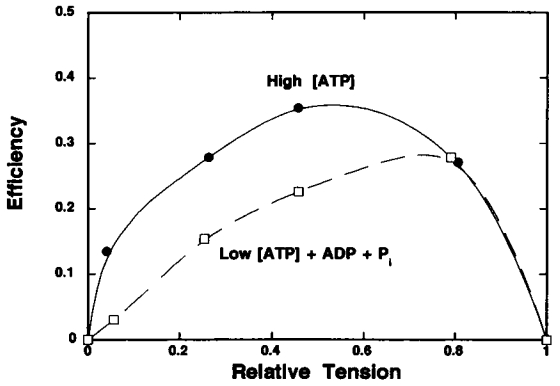

FIGURE 10 Efficiency of isotonic shortening. Efficiency was calculated as work done during isotonic shortening divided by the free energy of ATP given in the text as Eq 3. Symbols: efficiency between ~800 and 400 μM [ATP] (●); efficiency between ~400 μM and 0 [ATP] (□).

$[ATP]_i$ + 300 μM, and $[ATP]_f$ was set to the equilibrium value, $3 \cdot 10^{-12}$ M. The reduced efficiency indicated by the lower curve in Fig. 10 indicates that the rigor (AM and AM.ADP) cross-bridges within the fiber during shortening waste some of the free energy transduced by other cross-bridges. This behavior is expected if the rigor cross-bridges form an internal load.

Interaction distance (D_i), interaction time, and ATPase cycle time

D_i is plotted vs. sliding velocity averaged over the initial high-ATP period of shortening in Fig. 11 *A*. D_i increased approximately linearly with the shortening velocity according to the relationship $D_i = mV + D_o$ (*solid line* in Fig. 11 *A*), where V is the shortening velocity. The intercept at zero velocity is 8.3 nm and the slope (m) is 27.1 ms. At 0.07 P_o load, the initial velocity of shortening at high [ATP] was 2.7 $\mu m \cdot s^{-1}$ and the average velocity between 700 and 400 μM ATP was 1.94 $\mu m \cdot s^{-1}$. However, the 700 μM ATP concentration liberated in the experiments was not sufficient to saturate the shortening velocity at low load (Fig. 5 *A*), implying that nucleotide-free cross-bridges exerted a significant internal mechanical load even in the high $[ATP_u]$ range. Thus the 60-nm D_i obtained between 700 and 400 μM $[ATP_u]$ underestimates the D_i that would be obtained in the absence of an internal load, such as at saturating [ATP]. At high [ATP] and zero external load, the filament sliding velocity is 6.8 $\mu m \cdot s^{-1}$. If the linear relationship between D_i and velocity extends up to higher velocities, the extrapolated value of D_i at 6.8 $\mu m \cdot s^{-1}$ is 193 nm.

Because D_i can be expressed as $V \cdot S_a \cdot [M_o]/J$, where J is the ATPase flux rate, it follows from the linear D_i vs. velocity relationship that the ATPase activity is given by

$$J = \frac{VS_a[M_o]}{D_i} = \frac{VS_a[M_o]}{mV + D_o}$$

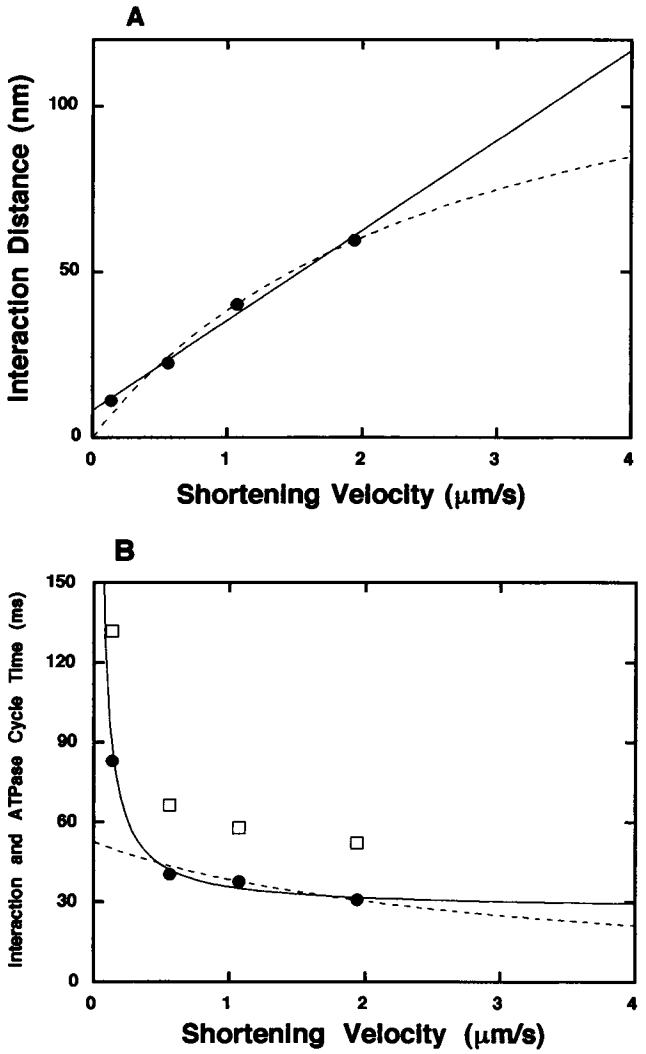

FIGURE 11 Interaction distance and time plotted against shortening velocity. Shortening velocity was calculated as the average of the initial velocities at high (~800 μM) [ATP] and low (~400 μM) [ATP] with added ADP and P_i. (*A*) Interaction distance at high [ATP]. The solid line represents a linear regression to the data, D_i (nm) = $27.1 \cdot V + 8.275$, r = 0.996, where V = shortening velocity in $\mu m \cdot s^{-1}$. The dashed line represents a saturating relationship of D_i vs. velocity, text Eq. 4, fitted to the data, D_i (nm) = $154 \cdot V/(2.93 + 1.09 \cdot V)$. (*B*) Interaction time per ATP molecule hydrolyzed by myosin heads interacting with actin filaments (●), calculated from interaction distance divided by shortening velocity, and ATPase cycle time (□), calculated from interaction time divided by relative stiffness.

This relationship between ATPase flux rate and shortening velocity saturates at high velocities, leading to D_i values that increase linearly with velocity.

Although the approximately linear dependence of D_i on velocity up to ~2 $\mu m \cdot s^{-1}$ shown in Fig. 11 *A* suggests that the ATPase flux saturates at high velocity, we do not actually have evidence for such a saturation. ATPase rate might increase with velocity and not saturate. If the cross-bridge attachment and detachment rates are given by f and g, respectively, then the ATPase flux rate is given by $J = f \cdot g/(f + g)$ and the proportion of cross-bridges attached is

given by $S_a = f/(f + g)$. The ratio J/S_a then gives the detachment rate, g. If g increases linearly with velocity ($g = J/S_a = g_o + q\,V$), then

$$D_i = \frac{VS_a[M_o]}{J} = \frac{V[M_o]}{g_o + qV} \quad (4)$$

This relationship (*dashed curve* in Fig. 11 *A*) fits the data at velocities $\geq 0.5\ \mu m \cdot s^{-1}$, but the point at the lowest velocity ($0.14\ \mu m \cdot s^{-1}$) is above the curve. Extrapolating the dashed curve to the maximum velocity ($6.8\ \mu m \cdot s^{-1}$) at zero load and at saturating [ATP] gives an estimate of 102 nm for the maximum interaction distance. Thus with reasonable assumptions about the behavior of J with velocity, the data suggest that in the absence of internal and external loads, D_i is in the range 100–190 nm.

The duration of actomyosin interaction per ATP molecule hydrolyzed (interaction time) can be obtained by dividing D_i by shortening velocity (Fig. 11 *B*, *closed circles*). Interaction time, divided by the stiffness, gives the ATPase cycle time (reciprocal of the ATPase rate) during shortening (Fig. 11 *B*, *squares*). Both interaction time and ATPase cycle time decrease markedly as velocity increases in the low velocity range, but at velocities $\gtrsim 1\ \mu m \cdot s^{-1}$, interaction time and the ATPase cycle time hardly change with velocity. This behavior can also be observed with intact frog muscle fibers, as discussed in the next section, from previously published data. The curves in Fig. 11 *B* indicate the interaction time if D_i increases linearly with velocity (*solid curve*) or if D_i saturates at high velocity (*dashed curve*). Experiments at higher [ATP] than used here will be required to determine D_i and ATPase cycle time at maximum velocity.

Relation to other studies

Sliding distance estimates greater than the length of the myosin head (16–19 nm, Elliott and Offer, 1978; Rayment et al., 1993) challenge the conventional hypothesis that force is generated when myosin undergoes a structural change such as a tilting motion while attached to actin and that myosin and actin interact once per biochemical ATPase cycle. Since Yanagida et al. (1985) reported that the sliding distance of crab myofibrils per ATP molecule utilized is ≥ 60 nm, several times larger than expected, there have been many reports on actomyosin sliding distance. In many of these studies, myosin or its fragments were bound to a microscope slide and fluorescent-labeled actin filaments were observed actively translating along the layer of myosin, an in vitro assay of motility termed the "myosin-coated surface assay." From the translation velocity, the ATPase rate, and the protein densities, the apparent sliding distance per ATP molecule utilized can be calculated. The term "step size," which has often been applied in this context, does not distinguish the elementary force-generating event from the total distance of filament translation produced by one ATPase cycle. We prefer the term "working stroke" to signify the filament sliding distance attained while the myosin head is producing positive sliding force.

Measurements using actomyosin in vitro have resulted in widely varying estimates for the sliding distance per biochemical cycle (Toyoshima et al., 1990; Uyeda et al., 1990, 1991; Harada et al., 1990). Among the uncertainties in these studies has been the number of heads working simultaneously on a minimal length of actin filament that is just long enough to support motion at nearly full speed, the effect of random orientation of the myosin molecules on the substrate, the relevant rate of ATP splitting, and the infrequent interaction between a myosin molecule and actin (reviewed by H. E. Huxley, 1990, and Yanagida, 1990). Studies of actin displacement generated by single myosin molecules have generally agreed that the elementary mechanical stroke is <20 nm (Finer et al., 1994; Ishijima et al., 1994), but these studies do not resolve whether one or several mechanical interactions accompany the biochemical cycle because ATPase rate was not measured.

Experiments on muscle fibers avoid some of these problems. The substrate utilization can be directly measured and the proportion of cross-bridges attached to actin during sliding can be estimated from the mechanical stiffness. The interaction distance measured in our study should be clearly distinguished from the working stroke that is estimated from the in vitro studies. Assuming that each cross-bridge contributes an equal increment to stiffness when it is attached, the D_i value includes all forms of cross-bridge attachment whether or not they generate positive force. The various types of cross-bridge attachment that may contribute to D_i are described in the next section.

In our previous paper (Higuchi and Goldman, 1991b) we measured a lower limit for D_i of 40 nm for sliding between ~700 μM and zero ATP. From analysis of D_i between ~700 and ~300 μM ATP to reduce the contribution of dragging cross-bridges at low [ATP], we obtained $D_i \geq 60$ nm. Here we confirmed those earlier values, and using reasonable assumptions about the dependence of ATPase flux on velocity, extrapolated the data to higher [ATP] and lower load giving D_i = 100–190 nm.

Mechanical and energetic data available in the literature for frog muscle fibers near 0°C can be assembled to estimate an equivalent D_i in that preparation. Take the half-sarcomere force-velocity curve to be $(P + a) \cdot (V + b) = (P_o + a) \cdot b$ with constants $a = 0.25\ P_o$, $b = a\ V_{max}/P_o$ and $V_{max} = 2.2\ \mu m \cdot s^{-1}$ per half sarcomere (Hill, 1938), the stiffness of the fiber during shortening relative to that in rigor to be $S_a = 0.32 + 0.48\ P/P_o$ (Ford et al., 1985 combined with Goldman and Simmons, 1977), the rate of ATP splitting per myosin head at maximal sliding velocity = $5.0\ s^{-1}$ (Kushmeric and Davies, 1969; Homsher et al., 1981), and the rate of energy utilization (relative to the product $P_o \cdot V_{max}$) to be $J/(P_o \cdot V_{max}) = 0.0625 + 0.16 \cdot V/V_{max} + 1.18\ P \cdot V/V_{max}$ (Hill, 1964). ATPase cycle time, calculated from the reciprocal of J, has a similar dependence on velocity as the solid curve in Fig. 11 *B*. The interaction distance, given by $D_i = S_a \cdot V/J$, varies with relative force

similarly to the data obtained in this study for rabbit fibers (*upper curve* in Fig. 9 *B*). The maximal D_i for the frog fiber data at zero force is 141 nm, a value within the 100–190 nm range obtained here for rabbit fibers extrapolated to high [ATP].

Working and drag contributions to D_i

During interaction with actin, myosin heads may produce positive or negative forces or both (A. F. Huxley, 1957). Inasmuch as the interaction distance is the total filament sliding during actomyosin interaction, D_i corresponds to the sum of the working stroke of cross-bridges producing positive force and the drag distance of cross-bridges producing negative force. At low sliding velocity (high force in Fig. 9 *B*) and at low [ATP] (Yamada et al., 1993), $D_i \cong 10$ nm, a value compatible with a single tilting motion (or other structural change) in the 16–19-nm–long myosin head. As load is reduced and velocity increases, the increase in D_i to ≥ 60 (Fig. 9 *B*) indicates an increase in the working distance or the drag distance or both. If the working distance remains <20 nm at high velocities, $D_i \geq 60$ implies a drag distance of ≥ 40 nm, and the extrapolated D_i values of 100–190 nm in Fig. 11 *A* imply drag distances of 80–170 nm. The working and drag distances represent average values so that the distances of some myosin heads are longer than the averages.

If myosin heads did not repeatedly attach to and detach from the actin filament during this negative force production, the heads or rod portions of the molecules would have to change their shape markedly to accommodate filament sliding. Electron micrographs, however, showed that the shape of myosin heads during active shortening is similar to that in isometric contractions (Tsukita and Yano, 1985, 1986). The resolution of the quick-freeze, acetone substitution method used in those electron micrographic studies is better than 10 nm (Hirose et al., 1993) so that such a 80–170 nm structural change should have been observed. Thus, if the working distance of a cross-bridge within one ATPase cycle is assumed to be <20 nm, it seems that myosin heads repeatedly attach to and detach from actin during an ATPase cycle, at least during the drag portion of D_i.

A problem with considering D_i at high velocity to be composed of only one 10–20 nm working stroke and a 80–170 nm drag stroke is that at V_{max}, forces of positively and negatively strained cross-bridges are balanced (A. F. Huxley, 1957). To obtain this force balance, the lengths of the working and drag strokes must be in the same range unless positively and negatively strained cross-bridges have the very different stiffness. However, stiffness of negatively strained cross-bridges does seem similar to that of positively strained ones (Goldman, 1987b; Goldman et al., 1988), which leads to the conclusion that the working distance is about the same as drag distance. Working distance at high velocity in this study then becomes ≥ 30 or 50–95 nm, values much greater than length of the head, suggesting that multiple force-generating attachment and detachment cycles occur during each biochemical cycle. Intermediates of the actomyosin ATPase cycle likely to contribute to the interaction distance are strongly bound force generating states such as AM′.ADP.P_i, AM′.ADP, and AM.ADP and weakly bound preforce states such as AM.ADP.P_i (Hibberd and Trentham, 1986; Goldman, 1987a; Dantzig et al., 1992).

Cooke et al. (1994) suggested that multiple attachment/detachment cycles could take place without excess energy utilization if the free energy liberated in the working stroke is recovered in a drag stroke. Such energetically neutral mechanical cycles would help explain the present high D_i values, but would not explain the high working stroke values obtained in some in vitro studies (Harada et al., 1990; Saito et al., 1994). Another difficulty with this interpretation is that the structural basis for efficient transfer of energy accumulated by a dragging cross-bridge into additional power strokes is uncertain. If free energy is stored in a mechanical compliance within the cross-bridge during sliding (e.g., elasticity of the myosin rod), then the protein motions associated with transfer of energy stored in compression of the elasticity (negative strain) to extension (positive strain) should be addressed. Such energy might be stored as the free energy of ionic or hydrophobic interactions between residues in the proteins rather than as mechanical energy.

Lombardi and Piazzesi (1990) and Piazzesi and Lombardi (1995) proposed a model, modified from those of A. F. Huxley (1957) and A. F. Huxley and Simmons (1971), which assumes that a myosin head can repeatedly attach to actin, generate force, and detach during a single turnover of the ATPase reaction. This model predicts that the force produced by a myosin head would display large and rapid fluctuations. Ishijima et al. (1991), however, showed that force production by groups of myosin heads fluctuates during isometric contraction but hardly at all during shortening. To obtain multiple elementary power strokes from splitting one ATP molecule, the free energy liberated would need to be metered out in small increments, partitioning free energy among states of either myosin or actin filaments. The structure of the intermediate energy states should be specified in a realistic model of this sort.

We thank E. Homsher and N. Millar for the gift of radioactively labeled caged ATP; V. Lombardi for supplying the moving-coil motor; J. Pili for excellent mechanical design and construction; and C. Cook, J. A. Dantzig, T. Funatsu, and M. Tokunaga for comments on an earlier version of the manuscript. The work was supported by National Institutes of Health Grant AR26846 to Yale E. Goldman and by the Muscular Dystrophy Associations of America.

REFERENCES

Blinks, J. R. 1965. Influence of osmotic strength on cross-section and volume of isolated single muscle fibres. *J. Physiol.* 177:42–57.

Cain, D. F., A. A. Infante, and R. E. Davies. 1962. Chemistry of muscle contraction. Adenosine triphosphate and phosphorylcreatine as energy supplies for single contractions of working muscle. *Nature.* 196:214–217.

Cecchi, G., F. Colomo, and V. Lombardi. 1976. A loudspeaker servo system for determination of mechanical characteristics of isolated muscle fibres. *Boll. Soc. Ital. Biol. Sper.* 52:733–736.

Cooke, R., and K. Franks. 1980. All myosin heads form bonds with actin in rigor rabbit skeletal muscle. *Biochemistry.* 19:2265–2269.

Cooke, R., H. White, and E. Pate. 1994. A model of the release of myosin heads from actin in rapidly contracting muscle fibers. *Biophys. J.* 66: 778–788.

Craig, R., A. G. Szent-Györgyi, L. Beese, P. Flicker, P. Vibert, and C. Cohen. 1980. Electron microscopy of thin filaments decorated with a Ca^{2+}-regulated myosin. *J. Mol. Biol.* 140:35–55.

Dantzig, J. A., Y. E. Goldman, N. C. Millar, J. Lacktis, and E. Homsher. 1992. Reversal of the cross-bridge force-generating transition by photogeneration of phosphate in rabbit psoas muscle fibres. *J. Physiol.* 451:247–278.

Elliott, A., and G. Offer. 1978. Shape and flexibility of the myosin molecule. *J. Mol. Biol.* 123:505–519.

Ferenczi, M. A., E. Homsher, and D. R. Trentham. 1984. The kinetics of magnesium adenosine triphosphate cleavage in skinned muscle fibres of the rabbit. *J. Physiol.* 352:575–599.

Finer, J. T., R. M. Simmons, and J. A. Spudich. 1994. Single myosin molecule mechanics: piconewton forces and nanometre steps. *Nature.* 368:113–119.

Ford, L. E., A. F. Huxley, and R. M. Simmons. 1977. Tension responses to sudden length change in stimulated frog muscle fibres near slack length. *J. Physiol.* 269:441–515.

Ford, L. E., A. F. Huxley, and R. M. Simmons. 1981. The relation between stiffness and filament overlap in stimulated frog muscle fibres. *J. Physiol.* 311:219–249.

Ford, L. E., A. F. Huxley, and R. M. Simmons. 1985. Tension transients during steady shortening of frog muscle fibres. *J. Physiol.* 361:131–150.

Goldman, Y. E. 1987a. Kinetics of the actomyosin ATPase in muscle fibers. *Annu. Rev. Physiol.* 49:637–654.

Goldman, Y. E. 1987b. Measurement of sarcomere shortening in skinned fibers from frog muscle by white light diffraction. *Biophys. J.* 52:57–68.

Goldman, Y. E., M. G. Hibberd, and D. R. Trentham. 1984a. Relaxation of rabbit psoas muscle fibres from rigor by photochemical generation of adenosine-5′-triphosphate. *J. Physiol.* 354:577–604.

Goldman, Y. E., M. G. Hibberd, and D. R. Trentham. 1984b. Initiation of active contraction by photogeneration of adenosine-5′-triphosphate in rabbit psoas muscle fibres. *J. Physiol.* 354:605–624.

Goldman, Y. E., J. A. McCray, and D. P. Vallette. 1988. Cross-bridges in rigor fibres of rabbit psoas muscle support negative forces. *J. Physiol.* 398:72 P.

Goldman, Y. E., and R. M. Simmons. 1977. Active and rigor muscle stiffness. *J. Physiol.* 269:55–57 P.

Goldman, Y. E., and R. M. Simmons. 1984. Control of sarcomere length in skinned muscle fibres of *Rana temporaria* during mechanical transients. *J. Physiol.* 350:497–518.

Gordon, A. M., A. F. Huxley, and F. J. Julian. 1966. Tension development in highly stretched vertebrate muscle fibres. *J. Physiol.* 184:143–169.

Griffiths, P. J., C. C. Ashley, M. A. Bagni, Y. Maéda, and G. Cecchi. 1993. Cross-bridge attachment and stiffness during isotonic shortening of intact single muscle fibers. *Biophys. J.* 64:1150–1160.

Hanson, J., and J. Lowy. 1963. The structure of F-actin and of actin filaments isolated from muscle. *J. Mol. Biol.* 6:46–60.

Harada, Y., K. Sakurada, T. Aoki, D. D. Thomas, and T. Yanagida. 1990. Mechanochemical coupling in actomyosin energy transduction studied by *in vitro* movement assay. *J. Mol. Biol.* 216:49–68.

Hibberd, M. G., and D. R. Trentham. 1986. Relationships between chemical and mechanical events during muscular contraction. *Annu. Rev. Biophys. Biophys. Chem.* 15:119–161.

Higuchi, H., and Y. E. Goldman. 1991a. Sarcomere shortening per ATP molecule released from caged ATP within rabbit skinned muscle fibers. *Biophys. J.* 59:A376.

Higuchi, H., and Y. E. Goldman. 1991b. Sliding distance between actin and myosin filaments per ATP molecule hydrolysed in skinned muscle fibres. *Nature.* 352:352–354.

Higuchi, H., and Y. E. Goldman. 1992. Sliding interaction distance in rabbit skinned muscle fibers. *Biophys. J.* 61:A140.

Higuchi, H., T. Yanagida, and Y. E. Goldman. 1995. Compliance of thin filaments in skinned fibers of rabbit skeletal muscle. *Biophys. J.* 69: 1000–1010

Hill, A. V. 1938. The heat of shortening and the dynamic constants of muscle. *Proc. R. Soc. Lond. B.* 126:136–195.

Hill, A. V. 1964. The effect of load on the heat of shortening of muscle. *Proc. R. Soc. Lond. B.* 159:297–318.

Hirose, K., T. D. Lenart, J. M. Murray, C. Franzini-Armstrong, and Y. E. Goldman. 1993. Flash and smash: rapid freezing of muscle fibers activated by photolysis of caged ATP. *Biophys. J.* 65:397–408.

Homsher, E., M. Irving, and A. Wallner. 1981. High-energy phosphate metabolism and energy liberation associated with rapid shortening in frog skeletal muscle. *J. Physiol.* 321:423–436.

Huxley, A. F. 1957. Muscle structure and theories of contraction. *Prog. Biophys. Biophys. Chem.* 7:255–318.

Huxley, A. F., and R. Niedergerke. 1954. Structural changes in muscle during contraction. *Nature.* 173:971–973.

Huxley, A. F., and R. M. Simmons. 1971. Proposed mechanism of force generation in striated muscle. *Nature.* 233:533–538.

Huxley, A. F., and R. M. Simmons. 1973. Mechanical transients and the origin of muscular force. *Cold Spring Harbor Symp. Quant. Biol.* 37:669–680

Huxley, H. E. 1969. The mechanism of muscular contraction. *Science.* 164:1356–1366.

Huxley, H. E. 1990. Sliding filaments and molecular motile systems. *J. Biol. Chem.* 265:8347–8350.

Huxley, H. E., and J. Hanson. 1954. Changes in the cross-striations of muscle during contraction and stretch and their structural interpretation. *Nature.* 173:973–976.

Huxley, H. E., A. Stewart, H. Sosa, and T. Irving. 1994. X-ray diffraction measurements of the extensibility of actin and myosin filaments in contracting muscle. *Biophys. J.* 67:2411–2421.

Irving, M., T. St. C. Allen, C. Sabido-David, J. S. Craik, B. Brandmeier, J. Kendrick-Jones, J. E. T. Corrie, D. R. Trentham, and Y. E. Goldman. 1995. Tilting of the light-chain region of myosin during step length changes and active force generation in skeletal muscle. *Nature.* 375: 688–691.

Ishijima, A., T. Doi, K. Sakurada, and T. Yanagida. 1991. Sub-piconewton force fluctuations of actomyosin *in vitro*. *Nature.* 352:301–306.

Ishijima, A, Y. Harada, H. Kojima, T. Funatsu, H. Higuchi, and T. Yanagida. 1994. Single-molecule analysis of the actomyosin motor using nanomanipulation. *Biochem. Biophys. Res. Commun.* 199:1057–1063.

Kensler, R. W., and M. Stewart. 1983. Frog skeletal muscle thick filaments are three-stranded. *J. Cell Biol.* 96:1797–1802.

Kojima, H., A. Ishijima, and T. Yanagida. 1994. Direct measurement of stiffness of single actin filaments with and without tropomyosin by *in vitro* nanomanipulation. *Proc. Natl. Acad. Sci. USA.* 91:12962–12966.

Kushmerick, M. J., and R. E. Davies. 1969. The chemical energetics of muscle contraction. II. The chemistry, efficiency and power of maximally working sartorius muscles. *Proc. R. Soc. Lond. B.* 174:315–353.

Lombardi, V., and G. Piazzesi. 1990. The contractile response during steady lengthening of stimulated frog muscle fibres. *J. Physiol.* 431:141–171.

Lovell, S. J., P. J. Knight, and W. F. Harrington. 1981. Fraction of myosin heads bound to thin filaments in rigor fibrils from insect flight and vertebrate muscles. *Nature.* 293:664–666.

Lymn, R. W., and E. W. Taylor. 1971. Mechanism of adenosine triphosphate hydrolysis by actomyosin. *Biochemistry.* 10:4617–4623.

Marston, S. B., and R. T. Tregear. 1972. Evidence for a complex between myosin and ADP in relaxed muscle fibres. *Nature.* 235:23–24.

Maw, M. C., and A. J. Rowe. 1980. Fraying of A-filaments into three subfilaments. *Nature.* 286:412–414.

Oosawa, F., and S. Hayashi. 1986. The loose coupling mechanism in molecular machines of living cells. *Adv. Biophys.* 22:151–183.

Piazzesi, G., and V. Lombardi. 1995. A cross-bridge model able to explain mechanical and energetic properties of shortening muscle. *Biophys. J.* 68:1966–1979.

Rader, C. M., and B. Gold. 1967. Digital filter design techniques in the frequency domain. *Proc. IEEE.* 55:149–171.

Rayment, I., W. R. Rypniewski, K. Schmidt-Base, R. Smith, D. R. Tomchick, M. M. Benning, D. A. Winkelmann, G. Wesenberg, and H. M. Holden. 1993. Three-dimensional structure of myosin subfragment-1: a molecular motor. *Science.* 261:50–58.

Reedy, M. K., K. C. Holmes, and R. T. Tregear. 1965. Induced changes in orientation of the cross-bridges of glycerinated insect flight muscle. *Nature.* 207:1276–1280.

Rüdel, R., and F. Zite-Ferenczy. 1979. Do laser diffraction studies on striated muscle indicate stepwise sarcomere shortening? *Nature.* 278: 573–575.

Saito, K., T. Aoki, T. Aoki, and T. Yanagida. 1994. Movement of single myosin filaments and myosin step size on an actin filament suspended in solution by a laser trap. *Biophys. J.* 66:769–777.

Tawada, K., and M. Kimura. 1984. Stiffness of glycerinated rabbit psoas fibers in the rigor state. *Biophys. J.* 45:593–602.

Thirlwell, H., J. A. Sleep, and M. A. Ferenczi. 1995. Inhibition of unloaded shortening velocity in permeabilised muscle fibres by caged-ATP compounds. *J. Muscle Res. Cell Motil.* 16:131–137.

Thomas, D. D., and R. Cooke. 1980. Orientation of spin-labeled myosin heads in glycerinated muscle fibers. *Biophys. J.* 32:891–906.

Toyoshima, Y. Y., S. J. Kron, and J. A. Spudich. 1990. The myosin step size: measurement of the unit displacement per ATP hydrolyzed in an *in vitro* assay. *Proc. Natl. Acad. Sci. USA.* 87:7130–7134.

Trentham, D. R., R. G. Bardsley, J. F. Eccleston, and A. G. Weeds. 1972. Elementary processes of the magnesium ion-dependent adenosine triphosphatase activity of heavy meromyosin. A transient kinetic approach to the study of kinases and adenosine triphosphatases and a colorimetric inorganic phosphate assay *in situ. Biochemistry.* 126:635–644.

Tsukita, S., and M. Yano. 1985. Actomyosin structure in contracting muscle detected by rapid freezing. *Nature.* 317:182–184.

Tsukita, S., and M. Yano. 1988. Instantaneous view of actomyosin structure in shortening muscle. *In* Molecular Mechanism of Muscle Contraction. G. H. Pollack and H. Sugi, editors. Plenum Press, New York. 31–38.

Uyeda, T. Q. P., S. J. Kron, and J. A. Spudich. 1990. Myosin step size: estimation from slow sliding movement of actin over low densities of heavy meromyosin. *J. Mol. Biol.* 214:699–710.

Uyeda, T. Q. P., H. M. Warrick, S. J. Kron, and J. A. Spudich. 1991. Quantized velocities at low myosin densities in an *in vitro* motility assay. *Nature.* 352:307–331.

Wakabayashi, K., Y. Sugimoto, H. Tanaka, Y. Ueno, Y. Takezawa, and Y. Amemiya. 1994. X-ray diffraction evidence for the extensibility of actin and myosin filaments during muscle contraction. *Biophys. J.* 67:2422–2435.

Walker, J. W., G. P. Reid, J. A. McCray, and D. R. Trentham. 1988. Photolabile 1-(2-nitrophenyl) ethyl phosphate esters of adenine nucleotide analogues. Synthesis and mechanism of photolysis. *J. Am. Chem. Soc.* 110:7170–7177.

Yamada, T., O. Abe, T. Kobayashi, and H. Sugi. 1993. Myofilament sliding per ATP molecule in rabbit muscle fibres studied using laser flash photolysis of caged ATP. *J. Physiol.* 466:229–243.

Yanagida, T. 1990. Loose coupling between chemical and mechanical reactions in actomyosin energy transductions. *Adv. Biophys.* 26:75–95.

Yanagida, T., T. Arata, and F. Oosawa. 1985. Sliding distance of actin filament induced by a myosin cross-bridge during one ATP hydrolysis cycle. *Nature.* 316:366–369.

Yates, L. D., and M. L. Greaser. 1983. Quantitative determination of myosin and actin in rabbit skeletal muscle. *J. Mol. Biol.* 168:123–141.